Projected changes in ENSO-driven regional tropical cyclone tracks

Submitted to Climate Dynamics March 2019

Revised December 2019

(Corresponding Author) Samuel S. Bell[1],

Savin S. Chand[1]

Christopher Turville[1]

Corresponding Author e-mail: ss.bell@federation.edu.au

[1] Centre for Informatics and Applied Optimization, Federation University Australia, Buninyong, VIC, Australia

Abstract

Simulations and projections of the El Niño Southern Oscillation's (ENSO's) influence on TC track variability was analysed globally using Coupled Model Intercomparison project Phase 5 (CMIP5) models. The ability of these models to simulate the historical (1970-2000) ENSO-TC track relationship and inform us of the likely projected changes resulting from high carbon emissions (RCP8.5) in a climate projection (2070-2100) was determined through cluster analysis. The number of seasonal TC occurrences during traditional ENSO events ("El Niño" and "La Niña") in each cluster were used to determine whether each cluster was "El Niño dominant", "La Niña dominant" or "neither". Only seven out of a combined total of twenty-eight clusters across all basins were found to disagree in terms of "ENSO dominance" between the observed records and historical model simulations. This suggests that models can simulate the ENSO and TC track relationship reasonably well. Under sustained high carbon emissions, La Niña TCs were projected to become dominant over El Niño TCs in the central South Indian Ocean (~60 – 100°E), the southern Bay of Bengal and over straight-moving TCs in the South China Sea. El Niño TCs were projected to increase and become dominant over La Niña TCs in a larger area of the western South Pacific (~160°E – 165°W) and central North Pacific (~160°E – 145°W) Oceans. Projections of track directions and lifetimes, while less robust, indicated that El Niño TCs would track westward more often in the Coral Sea (150 – 165°E), while El Niño TCs that took an eastward track here would have longer lifetimes (~3 days).

1. Introduction

The El Niño Southern Oscillation (ENSO) is a major driver of tropical cyclone (TC) activity at interannual timescales in different TC basins around the globe (e.g., Chu et al. 2004). In particular, the observed relationships between ENSO and TC genesis (e.g., Nicholls 1979; Gray 1984; Chan 1985; Chia and Ropelewski 2002; Kuleshov et al. 2009; Kim et al. 2011; Magee et al. 2017), tracks (Irwin and Davis 1999; Camargo et al. 2007c; Camargo et al. 2008; Kossin et al. 2010; Ramsay et al. 2012; Caron et al. 2015; Patricola et al. 2018) and intensity (Camargo and Sobel 2005; Frank and Young 2007; Chand and Walsh 2011) have received considerable scientific attention in the past. However, only a few studies have documented the extent at which state-of-the-art climate models are able to simulate the ENSO-TC relationship (e.g., Bell et al. 2014; Zhang et al. 2016a,b; Chand et al. 2017; Patricola et al. 2018; Tan et al. 2019), with the impact of climate change on this relationship explored by only a couple of these studies. Both Chand et al. (2017) and Tan et al. (2019) used CMIP5 models to explore the relationship between ENSO and TC genesis in a changing climate, though the latter was restricted to the western North Pacific Ocean, while Chand et al. (2017) explored this relationship globally (see also an up-to-date review on this subject by Lin et al. 2019). The present study seeks to build upon the prior work of Chand et al. (2017) but with an emphasis on TC tracks.

Representation of ENSO in modern-day climate models has improved over the past decade (Bellenger et al. 2014; Capotondi et al. 2015), although some aspects remain problematic to simulate, including certain climate feedback processes (Bellenger et al. 2014; Bayr et al. 2018). There is also evidence to suggest that some improvements in model skill are occurring due to error compensation rather than correct simulation of climate processes (Bellenger et al. 2014; Bayr et al. 2018). Nevertheless, these investigations have led to improvements in our understanding of the likely changes in ENSO conditions as a result of global warming. For example, a number of studies have indicated a projected increase in the frequency of non-conventional (central Pacific or "warm pool") El Niño events compared to more traditional (eastern Pacific or "cold tongue") El Niño events in the future climate (e.g., Yeh et al. 2009; Collins et al. 2010; Kim and Yu 2012). It is important to note that as climate models are not able to adequately simulate the effects of non-conventional ENSO events (Power et al. 2013; Taschetto et al. 2014), we do not discriminate between traditional and non-traditional ENSO events or different stages of ENSO development (e.g., onset and decay, Chu et al. 1997; Jin et al. 2014; Lin et al. 2019) in this study.

The frequency of extreme El Niño events has also been projected to increase (Cai et al. 2014) due to global warming. Furthermore, some studies have suggested a likely weakening of the "Walker" circulation in response to global warming, thus giving rise to more "El Niño-like" conditions in the future (Vecchi and Soden 2007; Christensen et al. 2013). Nevertheless, there is a very high expectation that ENSO will continue to dominate regional-scale climate variability in the future (Christensen et al. 2013; Power et al. 2013) and strongly influence weather-related variables such as rainfall (Power et al. 2013) and TCs (Chand et al. 2017) in a changing climate.

Chand et al. (2017) showed robust future changes in ENSO-driven variability in TC frequency and genesis locations in the Pacific, and elsewhere around the globe, in response to global warming. Our present study extends the work of Chand et al. (2017) to examine regional-scale changes in TC tracks as a result of future changes in ENSO variability. This gives insight into how TC tracks, and resulting TC impacts through landfalling events, will change as a result of the changing nature of ENSO in a warming climate. The independent tracking and detection scheme of Tory et al. (2013a), that circumvents dependence on model tuning, is applied to detect and track TCs in Coupled Model Intercomparison Project Phase 5 (CMIP5; Taylor et al. 2012) models of medium to coarse resolution. Although TC intensities are poorly resolved in these models (e.g., Davis 2018), the genesis location and track of high intensity TCs have been realistically simulated by the Tory et al. (2013a) scheme in reanalysis data at a similar horizontal resolution as these models (Tory et al. 2013b). Models for each basin are selected based on their overall performance in that basin while model autocorrelation (e.g., Knutti et al. 2013; Sanderson et al. 2015) is removed in our model selection process. Once selected, detected TCs from each model are respectively combined to form multi-model means for the two simulation periods: a historical simulation over the period 1970-2000 and a climate projection over the period 2070-2100 under a high radiative forcing of RCP8.5 (see Section 2b).

A popular method for isolating similar track types in a given TC basin is via a clustering algorithm, particularly the curve-clustering algorithm of Gaffney et al. (2007) that treats each TC track as a mathematical function to accommodate tracks of different shapes and sizes. This clustering algorithm has been used extensively on observational TC track data in different TC basin around the globe. The definitions of these basins are mostly retained in our study as well for consistency: the Southern Hemisphere (Ramsay et al. 2012) that includes the South Indian Ocean, the Australian region and the South Pacific Ocean, the North Indian Ocean (NI) basin (Paliwal and Patawarthan 2012), the Western North Pacific (WNP) basin (Camargo et al. 2007a,b), the Eastern North Pacific (ENP) basin (Camargo et al. 2008; Caron et al. 2015) and the North Atlantic (NA) (Kossin et al. 2010; Kozar et al. 2012; Boudreault et al. 2017). However, analysing TC tracks in climate models requires a slightly different approach because models often detect TCs in regions where they do not occur in reality. This leads to the use of additional clusters in some regions (e.g., Ramsay et al. 2018). Furthermore, fundamental differences between the observed and model-detected tracks (such as different track shapes and lifetimes) make it better practice to cluster all tracks together in one large set. Resultant TC tracks can be then re-grouped into their original source of data (i.e., observed records, historical and RCP8.5 simulations) post-clustering, and hence the frequency differences between these sets of data in regional clusters can be established. Each TC track in a given regional cluster may be associated with a specific phase of ENSO (i.e., El Niño or La Niña). Considering many TC tracks over many years of data, the relative ENSO-dominance of specific clusters can be determined. It can then be established objectively how well such ENSO-cluster relationships are simulated in models and how they are likely to change in response to global warming.

The outline of this paper is as follows. Section 2 gives an overview of data, definitions and methods used in the study. Section 3 provides assessments and discussions of the ENSO-TC track relationship in different TC basins around the globe, including assessments of historical and RCP8.5 climate model simulations and associated changes in large-scale environmental mechanisms that affect TC activity. Finally, section 4 gives a summary of the major findings of this work.

2. Data, Definitions and Methods

a. Observational data

The best-track dataset compiled in the International Best Track Archive for Climate Stewardship (IBTrACS-WMO, Knapp et al. 2010) is used in three of our five basins (Table 1). The best-track data in these basins strongly compare with those detected in ERA-Interim reanalysis data set (e.g., Bell et al. 2018). However, due to inconsistencies between the NI TC observations (IBTrACS-WMO) and those detected in reanalysis/climate model data (e.g., Strachan et al. 2013; Tory et al 2013c; Bell et al. 2018), we instead use TCs detected in ERA-Interim reanalysis data in place of observations for the NI Ocean basin. For the WNP basin, the Joint Typhoon Warning Centre (JTWC, 2017) dataset is used.

For consistency, TC tracks in all observed records were defined to be consistent with tracks detected in climate models (see Section 2d). Observed TC tracks begin at a position when a storm first reaches the 10-minute sustained wind speed of 17 m s^{-1}, with those storms not reaching this intensity excluded from the analyses. Observed tracks are terminated in two cases: (1) if a forecast centre no longer tracks them (i.e., track information ceases in the database) or (2) if they encounter an objectively diagnosed subtropical jet[2] as they move poleward (Tory and Dare 2015); the subtropical jet criteria isolates TCs from those that may form as non-tropical systems in the sub-tropics.

b. CMIP5 model data

Single ensemble runs from thirteen different models from the Coupled Model Intercomparison Project (CMIP5, Taylor et al. 2012) that performed well in prior studies in terms of simulating TC formation climatology (Tory et al. 2013c), ENSO (Bellenger et al. 2014) and ENSO-TC characteristics (Chand et al. 2017) are used to create independent multi-model means for each TC basin (Table 2). In other words, TC outputs from several models are combined, and then averaged over the number of models for computations of TC frequency, track density and large-scale variables. Model selection for each basin was based on several factors including:

1. Model independence (e.g., Knutti et al. 2013)
2. Realistic number of TC detections (e.g., Bell et al. 2018; Bell et al. 2019a)
3. Realistic TC track trajectories (e.g., Bell et al. 2018; Bell et al. 2019a)

This resulted in the WNP having seven models, the NI four models, and the other regions having five models each. The CSIRO-Mk3.6 best met the criteria and was used in the multi-model mean for each basin except for the NI, while GFDL-ESM2M was not used in any multi-model mean. Note these rigorous model evaluation procedures have also removed models with strong biases in simulating ENSO-TC characteristics, thus giving more confidence in our projection results (e.g., Chand et al. 2017).

[2] This criterion is not available before 1979 (ERA-Interim start-date; Dee et al. 2011) and so data preceding this year was only used for the ENP and NA basins, due to little to no subtropical activity in the ENP (e.g., Romero-Vadillo 2008), while results for the NA basin were unaffected.

The following large-scale environmental genesis parameters (e.g., Camargo et al. 2007c, Murakami et al. 2010) were also used to construct multi-model means:

1. Upward velocity (omega at 500 hPa)
2. Relative humidity at 700 hPa
3. Vertical wind shear between 850 and 200 hPa
4. Relative vorticity at 850 hPa

For the Northern Hemisphere, these environmental parameters were averaged over the three-month period July to September, except for the NI basin, where the three-month period October to December was used; generally coinciding with peak TC activity in each TC basin. For the Southern Hemisphere, environmental parameters were averaged over the three-month period December to February.

The two climate scenarios assessed in this work are (1) a historical simulation over the period 1970 – 2000 to evaluate and assess climate models' ability to reproduce observed TC-ENSO climatology, and (2) a RCP8.5 projection (2070 – 2100) to determine any projected changes in the ENSO-TC track relationship as a result of global warming. Note that CMIP5 projections are often implemented with one of several Representative Concentration Pathways (RCP, Van Vuuren 2011) to control the level of carbon emissions in the atmosphere compared to pre-industrial times. In this study, the RCP8.5 that represents a maximum 8.5 W m^{-2} likely increase in radiative forcing over pre-industrial levels (Riahi et al. 2011) was chosen to best elucidate any changing TC-ENSO behaviour in a warmer climate (e.g., Chand et al. 2017).

c. Detection and tracking

The Okubo-Weiss-Zeta (OWZ) TC detection and tracking algorithm (Tory et al. 2013a) is used in this study to detect and track TCs in all models without any adjustment of thresholds to accommodate different model resolutions. The OWZ algorithm has undergone scrupulous validation in reanalysis data in terms of annual TC numbers and genesis positions (Tory et al.

2013b), and more recently in terms of tracks (Bell et al. 2018). Key details of the OWZ algorithm are provided in Tory et al. (2013a) while a good summary of the algorithm can be found in the Appendix of this paper. Crucially, the track validation study in Bell et al. (2018) identified a limitation in the algorithm, suggesting that those TCs lasting less than 2-days after declaration should be discarded for optimal performance. This study implements this suggestion by removing all such detected TCs.

d. TC track definition in models

The objective definition of a TC track established in Bell et al. (2018) is also used in the present study. This definition states that a TC track detected by the OWZ algorithm commences from the TC declaration location (as this location best matched the timing of a TC first reaching the 10-minute sustained wind speed of 17 m s^{-1} in the IBTrACS database) and terminates when a TC either dissipates or encounters an objectively diagnosed subtropical jet, which is identified in the reanalysis and model data by 200 h Pa jet steams >25 m s^{-1} and zonal winds exceeding 15 m s^{-1} (see Tory and Dare 2015 for details).

e. Cluster analysis

The probabilistic curve-clustering technique of Gaffney et al. (2007) is applied to group together TC tracks of similar properties in each basin. An advantage of clustering TC tracks is that different track types that overlap, particularly in the WNP, can be analysed separately. Each cluster analysis was run with all track data (observations, historical climate model simulations and RCP8.5 climate model projections) combined. This has the implicit advantage of binning different model and observed TC tracks into the same set of clusters. Some drawbacks of this method include potential contamination of model biases with observed climatology with model biases and heavily weighting individual clusters on model tracks. These drawbacks can impact on the geographic location of clusters. Steps were taken to reduce this impact by introducing more clusters to some regions and ensuring cluster arrangements were as close as possible (in terms of genesis location and track direction) to clusters identified in observation-only studies.

Twenty-five cluster runs were performed in each region where the input order of the tracks was randomized and 12 expected maximization (EM) starts were used. For each region, the cluster run with the smallest trained log-likelihood value was selected. Linear regression mixture (lrm) models were fitted to TC tracks with an objectively determined number of clusters, *k.* The chosen *k* for each region can be found in Table 3, noting some regions contain additional clusters as opposed to the prior observation-only based studies in order to account for unrealistic geographical regions of TC detections in models (see Tory and Ye 2018 for further reading).

f. Characterising ENSO phases

Conventionally, ENSO phases are defined in accordance with Niño indices that use sea-surface temperature (SST) anomalies averaged over the equatorial Pacific as proxies for the current state of ENSO (e.g., Trenberth 1997). However, classifying ENSO events in models can be challenging, as models contain spatial SST biases. Defining model-specific ENSO classifications to take into account model biases introduces subjective decisions that would make comparisons between models and observations more difficult (Taschetto et al. 2014). Here we adopt a method similar to Grose et al. (2014) that utilizes the standard deviations, σ, of the Niño 3.4 index (i.e., area averaged SST anomalies over the region 5°N-5°S, 120-170°W, hereafter N34) to classify ENSO into El Niño and La Niña events. As in Chand et al (2017), the $\pm 0.5\sigma$ threshold is chosen here as it gave the best statistical match (at 95% significance level) between ENSO events calculated from HadISST data and the observed records for the period 1970 to 2000. Note that the Niño 3.4 index used here can collectively define conventional ENSO-events as well as ‘Modoki El Niños’ (sometimes referred to as central

Pacific El Niños). For the purpose of this study, we do not seek to distinguish between different types of El Niños and their impacts on TCs, as most CMIP5 models still have biases and deficiencies in realistically simulating the observed structure of 'Modoki-type' events (Power et al. 2013; Tacshetto et al. 2014) as opposed to simulating conventional El Niños where CMIP5 models have improved substantially (Power et al. 2013; Bellenger et al. 2014; Murphy et al. 2015; Grose et al. 2014). Nevertheless, it is important to emphasise that 'Modoki' and conventional El Niño events can have different impacts on TCs in the Pacific (e.g., Wilks 2006; Hong et al. 2011; Chand et al. 2013a,b; Patricola et al. 2016; Magee et al. 2017; Patricola et al. 2018; Wu et al. 2018). Furthermore, at a time when representation of non-conventional ENSO events in climate models have improved, more sophisticated indices such as the E and C indices (e.g., Takahashi et al. 2011; Ren and Jin 2011) should be utilised in climate projection studies.

g. Isolating ENSO-related track clusters

In the Southern Hemisphere, a TC season is defined from July to June and is referred to in the overlapping year format (e.g., 1980/81). Each TC season may be classified as either El Niño ($N34 \geq 0.5$) or La Niña ($N34 \leq -0.5$) where the N34 index is based on the normalised standard deviation of the 3-monthly mean of a typical peak TC season (December, January and February, DJF). In the Northern Hemisphere, a TC season is defined from January to December and is referred to simply by that year. El Niño and La Niña years in the Northern Hemisphere are defined using the standardised SST anomalies for the months of July, August and September (JAS) as TC activity generally peaks during these months. Each TC track for different models are then binned into their respective ENSO phases that existed during that year.

In order for a cluster to be classified as either "El Niño dominant" or "La Niña dominant", there must be a statistically greater mean number of seasonal TCs in one phase over another. Using 10,000 bootstrap resamples, the mean number of TCs occurring in El Niño and La Niña years are calculated: an ENSO phase is considered dominant if the mean number of TCs are different under the U-test with 90% confidence (see Chu and Wang 1997 for details). Phases were also considered dominant if there was no overlap between resampled 95% confidence intervals of TC frequency.

3. Results

TC tracks from the observed records and the historical multi-model-mean simulations are first compared globally to provide a visual assessment of the relative performance of models in simulating ENSO-TC characteristics in different basins (Fig. 1a-f). Overall, it is clear that typical changes in TC activity due to ENSO variability are well-simulated in most basins. This includes for example, an enhancement (suppression) of TC activity north-eastward in the South Pacific Ocean during El Niño (La Niña) (e.g., Basher and Zheng 1995), as well as north-westward displacement of TCs in the WNP during La Niña (e.g., Chan 1985, 2000). Storm tracks reaching farther poleward in the western South Indian Ocean (~75°E) during El Niño events (Ho et al. 2006) are also apparent in the historical climate simulation (Fig. 1f). However, there are some exceptions that include, for example, simulation of the westward-eastward (El Niño-La Niña) shift in the ENP (e.g., Gray and Sheaffer 1991; Collins and Mason 2000). The historical model mean appears to overly simulate La Niña dominance over El Niño TCs too far west to 150°W (Fig. 1f) in comparison to the observations (Fig. 1c).

Similarly, a snapshot of the projected changes in TC track density between the historical and RCP8.5 (Fig. 1g,h) climate simulations for the two phases of ENSO (Figs 2a and 3a) provide an indication that some basins, such as the central Pacific region, are likely to have enhanced TC occurrences under RCP8.5 El Niño conditions compared to historical El Niño conditions. In other regions, such as the South Indian basin and eastern ENP, there are signs of suppressed TC activity. This suppression is consistent between both ENSO phases.

Underpinning these changes in terms of TC frequency are the changes in TC-relevant large-scale environmental fields (Figs 2b-e and 3b-e). For example, it is clear that all large-scale variables become less favourable (blue shading) for TC formation during El Niño events in the South Indian basin. Another interesting result is a projected poleward shift of TC activity near the equator in the North Atlantic Ocean. This result also appears to be consistent between both ENSO phases.

In addition, our results indicate an overall decrease in tropical mean upward vertical velocity (Figs 2b and 3b) under the RCP8.5 condition (approximately 31×10^{-4} Pa s^{-1} for the Southern Hemisphere and 5×10^{-4} Pa s^{-1} for the Northern Hemisphere), consistent with other global warming studies (e.g., Held and Soden 2006; Vecchi and Soden 2007). This is also consistent with the projected TC frequency change we find in respective hemispheres: an approximate decrease of 24% in the Southern Hemisphere and 3.5% in the Northern Hemisphere, again consistent with prior studies (e.g., Sugi et al. 2012; Held and Zhao 2012; Walsh et al. 2015).

Moving forward, in order to have a more comprehensive understanding of regional-scale TC track distributions and ENSO-TC relationships in the observed records and climate models, and to better interpret likely projected changes in the RCP8.5 simulation, we examine each basin separately using a TC track-clustering technique. The cluster analysis, as highlighted earlier in Section 2e, separates TC tracks into distinct groups (or clusters) based on TC track shape and geographical locations, and hence can provide a measure of how particular track types may change at a regional scale in response to global warming.

a. Southern Hemisphere

TC tracks in the Southern Hemisphere have a strong relationship with ENSO (as shown by a number of studies in the past e.g., Hastings 1990; Basher and Zheng 1995; Ramsay et al. 2012 and others). However, whether this relationship is likely to change in the future climate in response to global warming – and if so, how – remains unclear. In this section, we first examine the ability of CMIP5 models to realistically simulate the ENSO-TC relationship for the entire Southern Hemisphere basin and then evaluate likely changes in TC track distributions under the RCP 8.5 projection for El Niño and La Niña events. Following Ramsay et al. (2018), TC tracks in the Southern Hemisphere are represented here by eight clusters labelled S1 to S8: the first three clusters (i.e., clusters S1-S3) are in the South Indian Ocean, clusters S4-S6 are in the Australian region and clusters S7 and S8 are in the South Pacific Ocean (Fig. 4i).

i. Comparisons of observed and model-simulated ENSO-TC climatology

The cluster-specific mean number of TCs in the two ENSO phases for the observed and historical model simulations, as indicated by their 95% confidence intervals, compare reasonably well with each other (Figs. 4a-h). However, an exception is S1 where models showed significant La Niña dominance in comparison to the observed records, where neither phase was found to be significantly dominant (Fig. 4a). Clusters S4 (west of Australia) and S8 (central South Pacific) in the observed records are dominated by TCs occurring during La Niña and El Niño events respectively and were well simulated by the models. The remaining clusters (S2, S3, S5, S6 and S7) showed no major differences in the mean number of TCs between the two ENSO phases in the observed records. This feature was also well captured by the model historical simulations.

It is apparent that some clusters display distinct eastward and westward motion (Fig. 4i; see also Bell et al. 2019a), noting track direction can be quite erratic around Australia and have been shown to be influenced by other natural modes such as the Madden-Julian Oscillation (Lavender and Dowdy 2016). The rates of eastward and westward motion were measured in each cluster (Table 4). We found that the models tended to overestimate the number of westward-directed tracks in regions in the South Pacific. This was particularly the case for S7 La Niña TCs (where 45% of TC tracks move westward compared to just 12% in observations) and S8 El Niño TCs (where 47% of TC tracks move westward compared to just 15% in observations).

The extent at which ENSO dominates westward and eastward TC motion in selected clusters (S3-S7, Table 5) were examined by U-Tests to determine the relative dominance of each ENSO phase. Results were variable between the models and the observed records, although only two sub-clusters differed in statistical significance level (S3-West and S7-West). Overall, the historical model simulations are generally doing well in capturing the large-scale observed ENSO-TC track relationship for El Niño and La Niña events in each cluster, providing a level of confidence in our results on ENSO-TC track projections for the Southern Hemisphere region (see below).

ii. Projection of the future ENSO-TC relationship

Overall, four of the eight clusters showed a significant change in the dominant phase of ENSO between the RCP8.5 and historical climate simulations (Fig. 4j): clusters S1-S3 in the South Indian Ocean and cluster S7 in the South Pacific Ocean. Cluster S1 had less TCs occurring during RCP8.5 La Niña events compared to historical La Niña events. This resulted in RCP8.5 La Niña TC numbers becoming similar to that of RCP8.5 El Niño TC numbers. For clusters S2 and S3, where neither of the ENSO phases were dominant in the historical simulation, we note that both of these clusters became dominated by La Niña events in the RCP8.5 projection. This is because El Niño TC numbers decrease more than La Niña TC numbers in these clusters, particularly in S3 where there was a large projected reduction in the mean number of El Niño TCs. This also causes the sub-cluster, S3-East, to become La Niña dominant under RCP8.5 (Table 5). These changes are supported by less favourable environmental conditions for TC development between 75°E and 100°E during RCP8.5 El Niño events compared with historical El Niño events (Fig. 2b-e). In particular, we note that relative humidity (Fig. 2c) becomes particularly unfavourable within the TC genesis contour of S3 during El Niño events, while there is a reduction of wind shear in S3 during La Niña events (Fig. 3d) that was not found during El Niño events (Fig. 2d).

In the Australian region, clusters S4-S6 showed no overall change in the dominant phase of ENSO between historical and RCP8.5 climate simulations. S4 was dominated by La Niña in both simulation periods while clusters' S5 and S6 remain ENSO-neutral over both periods. However, there was a change in the S6-West sub-cluster that became El Niño dominant (from neither phase dominating) in the RCP8.5 projection (Table 5). Putting this result in the context of S6 TC frequency projections [which remain quite stagnant (Fig. 4f)] and westward/eastward ratio projections [where the El Niño ratio shifts in favour of westward TCs, and to a lesser extent La Niña shifts in favour of eastward TCs, (Table 4)] suggests El Niño TCs forming in the S6 region will be more likely to track westward under RCP8.5; though it is beyond the scope of this study to present a possible mechanism for this change.

Cluster S7 in the South Pacific was projected to become El Niño dominant under the RCP8.5 condition, with Fig. 4g indicating likely increases (decreases) in El Niño (La Niña) TC numbers respectively. Increased wind shear (Fig. 3d) and decreased upward velocity (Fig. 3b) are consistent with reduced TC numbers during La Niña events. During El Niño events, conditions within the S7 contour are mostly less favourable to TC formation (Fig. 2b-e), in contrast to a projected increase in TC numbers (Fig. 2a). Chand et al. (2017) hypothesized that a weakening of SST gradients would expand convective zones towards the south-west in the S7 region during El Niño events, consistent with more favourable large-scale conditions below the S7 contour (Fig. 2b-e). Farther into the eastern Pacific, the El Niño dominance of the S8 region was projected to continue under the RCP8.5 condition. Changes in large-scale conditions were mostly similar here between the two ENSO phases.

Changes to normalized TC track density in each cluster, where the number of TCs between RCP8.5 and historical simulations are held fixed, were also analysed with respect to

El Niño and La Niña events (Fig. 5). While some changes appear very noisy (e.g., S1), some useful information can be gathered from these figures. Notable changes included an increased tendency of El Niño TCs in the central South Indian (S3) to track westward rather than eastward (Fig. 5e) consistent with results in Table 4, while La Niña TCs appeared to shift farther poleward while retaining a similar track shape (Fig. 5f). Poleward shifts were also noted for both phases of ENSO off the Western Australian coast (S4, Fig. 5 g-h). Interpretations of density changes to the north and east of Australia were not as clear (S5-S7). In the central Pacific (S8), RCP8.5 El Niño TCs appeared more likely to form near the dateline (i.e., shift west) compared to historical El Niño TCs (Fig. 5o). In contrast, RCP8.5 La Niña TCs appeared more likely to form farther east compared to historical La Niña TCs (Fig. 5p).

Finally, changes in mean TC lifetimes between RCP8.5 and historical climate El Niño and La Niña events were computed for each cluster (Table 6), and for the cases of clusters S3-S6, computations were done for both "westward" and "eastward" TC tracks. The only case where there was a statistically significant difference (at the 95% significance level) between RCP8.5 and historical TC track lifetimes was for eastward TCs in S6 that underwent an increase during El Niño events (~3 days). The reason for this increase is unclear but it could potentially be related to TCs moving farther poleward (e.g., Sharmila and Walsh 2018) or a slow-down of TC translational speed (e.g., Kossin 2018).

b. North Indian

TC tracks in the NI basin are represented by four clusters, labelled NI1-NI4 (Fig. 6i). NI1 and NI2 exist within the Arabian Sea while NI3 and NI4 cover the Bay of Bengal. TC activity in this basin is strongly modulated by the powerful Asian monsoon, exhibiting a double peak associated with a pre-monsoon (May–June) and post-monsoon (October–December) season (e.g., Singh et al. 2001; Evan and Camargo 2011; Wahiduzzaman et al. 2017). ENSO's effects on NI TCs is unclear (e.g., Li et al. 2016). However, as ENSO matures towards the end of a calendar year, it can impact on TCs during the post-monsoon season (Ng and Chan 2012; Girishkumar and Ravichandran 2012).

Like for the Southern Hemisphere basin, we first evaluate the ability of climate models to simulate the observed ENSO-TC track relationship and then determine potential changes to this relationship due to global warming. We also included assessments restricted to just the post-monsoon (Oct-Dec) months. Note that due to inconsistencies in the best-track data for this basin, we instead used TCs detected in the ERA-Interim reanalysis to form a basis of comparison with historical climate model simulations (see Methods).

i. Comparisons of observed and model-simulated ENSO-TC climatology

Overall, the mean number of TCs in El Niño and La Niña phases of all clusters (over the entire season, i.e., Jan-Dec) compare well between the ERA-Interim and historical climate model simulations (Fig 6a-d), except for the northern Arabian Sea cluster (NI2), which unexpectedly showed dominance of La Niña in ERA-Interim. Given the relatively low number of TCs that occur in the Arabian Sea, investigations at timescales longer than 25-years may assist in confirming this relationship (e.g., as in Evan and Camargo 2011). In the remaining clusters, the ENSO phases did not show any dominance of the ERA-Interim TCs, as was found in the historical model simulations. Considering TCs from the post-monsoon season only, cluster NI4 (Fig. 6h) showed evidence of La Niña dominance in ERA-Interim, consistent with an eastward shift and more favourable conditions observed over the Bay of Bengal during La Niña events (Ng and Chan 2012; Girishkumar and Ravichandran 2012). However, climate models were unable to simulate this pattern of variability. We next examine whether any of the clusters may be affected by future changes in ENSO conditions in response to global warming.

ii. Projection of the future ENSO-TC relationship

There were no projected changes in the relative dominance of the ENSO phases between the

RCP8.5 and historical climate simulations in any of the four NI clusters for the January-December periods (Fig. 6a-d). However, one of the four clusters (i.e., cluster NI3) did show a significant difference in ENSO dominance between the RCP8.5 and historical climate simulations during the post-monsoon season (Fig. 6g). Unlike La Niña TCs, the El Niño TCs were reduced leading this cluster to become dominated by La Niña in the RCP8.5 climate. This may be related to a reduction in relative vorticity in the Southern Bay of Bengal region during RCP8.5 El Niño events (Fig. 2e), though a similar reduction is observed during La Niña events (Fig. 3e).

Differences in track density were also examined in each cluster during different ENSO phases (Fig. 7). For NI4, both phases of ENSO were found to contribute to enhanced exposure to the northern Bay of Bengal (Fig. 7g,h), noting a potential eastward shift during future El Niño events. Finally, changes in TC lifetime between RCP8.5 and historical El Niño and La Niña events were also computed for each NI cluster (Table 7). No statistically significant differences between RCP8.5 and historically simulated TC tracks were found.

c. Western North Pacific

TC tracks in the WNP exhibit significant modulation by ENSO in the observed records (e.g., Camargo et al. 2007b; Patricola et al. 2018). We note that while several past projection studies in this basin have been dedicated to TC track projections (e.g., Wang and Wu 2011; Colbert et al. 2015), only a recent study by Tan et al. (2019) considered the impact of ENSO. Tan et al. (2019) cited a lack of robustness in their results, flagging underestimations of both ENSO's impact and TC genesis frequency. Thus, this work which implements a fundamentally different detection scheme, makes an important contribution to the world's most active TC basin in furthering our understanding of how future changes in ENSO may influence TCs and TC track characteristics in this basin. TC tracks are represented by nine clusters, labelled W1-A to W9-I (letters are also used to label clusters in the WNP to be consistent with prior studies). The clusters are numbered in order from the highest to lowest TC frequency across the study region (Fig. 8).

i. Comparisons of observed and model-simulated ENSO-TC climatology

The six most populous of the nine clusters showed a similar degree of modulation by the two ENSO phases between the observed records and historical simulations as indicated by their 95% confidence intervals (Fig. 8a-i); clusters W7-D, W8-G and W9-I were the exceptions. Each of these clusters in the historical simulations showed El Niño dominance in comparison to the observations where neither phase was found to dominate. It is noted in other studies (e.g., Camargo et al. 2007b) that observed TCs in cluster W1-A can be substantially enhanced during La Niña conditions. However, it is clear that the models were unable to simulate any hint of La Niña dominance in this cluster (Fig. 8a). Apart from these inconsistencies, ENSO modulation in the remaining clusters was well simulated, and overall satisfactory over the entire WNP basin. In the next section, we examine whether any of the clusters are likely to be affected by future changes in ENSO conditions in response to global warming.

ii. Projection of the future ENSO-TC relationship

Three of nine clusters showed a significant difference in ENSO dominance between the RCP8.5 projection and historical climate simulation (Fig. 8f,g,i). All of these changes in dominance occurred in straight-moving clusters in or near the South China Sea (W6-H, W7-D and W9-I). Each of these clusters contained less El Niño TCs in the RCP8.5 simulation than the historical simulation, accounting for changes in ENSO dominance.

Projected decreases of TC activity during El Niño events in the southwestern segment of the basin (e.g., straight-moving clusters of W3-B, W7-D, W9-I and to less extent W6-H) are difficult to attribute to changes in large-scale environmental conditions. Upward motion and relative vorticity did become less favourable inside W6-H’s genesis contour (Fig. 2b,e).

However, there was no clear decreases in favourability inside the more populous TC cluster contours (W3-B and W7-D). This leads us to conclude that this may be more of a change in track rather than environmental genesis conditions. Indeed, prior studies have indicated more TCs taking a northwestward (recurving) track under RCP8.5 (e.g., Colbert et al. 2015), especially during El Niño events. Such tracks are likely to be binned into nearby recurving clusters such as W1-A and W2-E instead. During La Niña events, relative humidity (Fig. 3c) and relative vorticity (Fig. 3e) become more favourable for TC formation over W9-I under RCP8.5, consistent with a slight increase in La Niña TC frequency shown in Fig. 8i. Overall, projected increases of TC activity are confined to the south-west of Japan during La Niña events (Fig. 3a) associated with reductions of vertical wind shear extending less east than during El Niño events (Figs 2c and 3c). Projected increases in TC activity during El Niño events in the northern (W5-F) and eastern (W8-G and to a lesser extent W4-C) segments of the basin are consistent with reduced wind shear (Fig. 2d) and increased upward motion (Fig. 2b) respectively. Relative humidity (Fig. 2c) is also increased over both these regions.

We note projected increases of TC frequency during La Niña in clusters W1-A and W5-F are minimal (Fig. 8a,e), indicating these tracks are likely traveling farther poleward (this is also likely the case during El Niño events; see also Fig. 9). There are many possible explanations as to why TCs may be traveling farther poleward here, they include (1) TCs are gestating farther poleward and therefore have more energy to sustain themselves (2) the environment is more favourable to sustaining TCs at higher latitudes i.e. “tropical expansion” or (3) the RCP8.5 TCs are more intense. It is difficult to quantify this exactly, though it is likely all three factors may have some role to play. Notably, TC track lifetimes in W5-F (insignificantly) increase irrespective of ENSO event (Table 7).

Differences in TC track densities for selected clusters were examined during El Niño and La Niña events (Fig. 9). Results indicate that La Niña TCs shift southwestward in W2-E and may have an increased tendency to track into Eastern China, consistent with a (statistically insignificant) increase of TC lifetimes in that cluster (Table 7). In the cluster that affects Vietnam and the Gulf of Thailand (W6-H), both El Niño and La Niña TC tracks shifted equatorward under the RCP8.5 condition (Fig. 9). An easing of vertical wind shear below the W6-H contour during El Niño events (Fig. 2d) was not present during La Niña events (Fig. 3d). Additional notable differences between RCP8.5 and historical track densities were for TCs in W5-F and W2-E with landfall over Japan appearing more likely in each of these except for W2-E during La Niña events (Fig. 9).

d. Eastern North Pacific

ENSO has been shown to have some influence on TC activity over the ENP basin, particularly toward the central Pacific where TC activity is increased during El Niño events (e.g., Chu and Wang 1997; Jien et al. 2015). TC tracks in the ENP are represented by 3 clusters, labelled E1 to E3 from left to right across the study region (Fig. 10d). TC numbers simulated by models were significantly underestimated off the coast of Mexico (E3, Fig 10c), possibly due to the crossing over land of low-pressure systems moving west from the Atlantic, which our detection system is not designed to accommodate (Bell et al. 2018).

i. Comparisons of observed and model-simulated ENSO-TC climatology

All three clusters in the ENP show similar modulation by the two ENSO phases between the observed records and historical climate simulations, as indicated by their 95% confidence intervals (Fig. 10a-c). Although no cluster was significantly dominated by either El Niño or La Niña TCs, visually, E1 (E2) is slightly El Niño (La Niña) dominant in the observed records consistent with shifts found by several TC-ENSO observational studies (Gray and Sheaffer 1991; Whitney and Hobgood 1997; Kimberlain 1999; Collins and Mason 2000). This pattern was well simulated by the models (Fig. 10a,b). In contrast, the apparent slight dominance of

La Niña TCs over El Niño TCs in E3 was not simulated well by the models, perhaps due to underestimation of model TCs in this cluster (Fig. 10c). In the next section, we examine whether any of the clusters are likely to be affected by future changes in ENSO conditions in response to global warming.

ii. Projection of the future ENSO-TC relationship

Two of three clusters showed a significant difference in ENSO dominance between the RCP8.5 and historical climate simulations (Fig. 10). Although E1 and E2 become El Niño and La Niña dominant in the RCP8.5 projection respectively, this is not a substantial change from the ENSO relationship in the historical climate simulation. Both El Niño and La Niña TCs were projected to increase in the central Pacific (E1) by a similar amount (Fig. 10a), which indicates the increase of TC activity west of 135°W in the central Pacific is not dependent on either phase of ENSO. This implies that projected increase in track density in the Hawaiian region (as noted in prior studies e.g., Murakami et al. 2013) can occur during both projected climate El Niño and La Niña events under the RCP8.5 condition (Fig. 11a,b).

In cluster E2, there was a marginal increase (decrease) in the mean La Niña (El Niño) TCs between historical and RCP8.5 climate simulations. This results in La Niña TCs becoming significantly more than El Niño TCs in the in the projected climate as opposed to the historical climate. Other than this, no major change was identified in this cluster. Like E1, we also note a marginal increase in track density contribution in E2 (from both El Niño and La Niña tracks) around Hawaii (Fig. 11c,d). Overall, a poleward shift in track density is projected for E1 and E2 El Niño TCs (Fig. 11a,c) and to some extent E2 La Niña TCs (Fig. 11d). Conversely, an equatorward shift in was projected for TCs forming close to the Mexican coast (E3) during both phases of ENSO (Fig. 11e,f). An equatorward formation shift is likely to push TC tracks farther away from the Mexican coastline, possibly decreasing the chance of landfall of TCs under RCP8.5. Large-scale conditions analysed in the ENP were largely consistent between both phases of ENSO (Fig. 2b-e; Fig. 3b-e), especially west of 110°W (i.e. inside the E1 and E2 contours). The only exception was a decrease of wind shear equatorward of the E2 and E3 75% genesis contours (red shading in Fig. 3d) during La Niña compared to El Niño events (Fig 2d). This was consistent with an equatorward shift in TC track density during RCP8.5 La Niña events (Fig. 11f).

e. North Atlantic

The NA basin experiences some modulation by ENSO, in particular more frequent TCs during La Niña events (e.g., Gray and Sheaffer 1991; Chu et al. 2004). TC tracks in the NA basin are represented by 4 clusters, labelled NA1 to NA4 from left to right across the study region (Fig. 12e). Several studies have documented the relatively poor performance of CMIP5 models in simulating realistic TC climatologies in this basin (e.g., Daloz et al. 2012; Tory et al. 2013c; Martin and Thorncroft 2015); and indeed, the clusters presented in this paper, that are strongly weighted on model tracks, are inconsistent with clusters found in observation-only studies (e.g., Kossin et al. 2010). Thus, we present projection results for the NA basin only briefly. TC numbers in cluster NA2 were too heavily underestimated by the models (Fig. 12b). So, additional bias-corrected intervals were computed ("grey-colored intervals" in Fig. 12b) by multiplying the original intervals by the ratio between the observed and historical intervals.

i. Comparisons of observed and model-simulated ENSO-TC climatology

Three of four clusters (NA1, NA2, and NA3) showed similar modulation by the two ENSO phases between the observed records and historical simulations, as indicated by their 95% confidence intervals (Fig. 12a-d). This included the models correctly simulating more TCs in the Gulf of Mexico (NA1) during La Niña events compared to El Niño events (Fig. 12a). Due to the very low number of observed TCs in NA3 and NA4, we note that the statistical test used was unable to provide an accurate distinction between ENSO dominance.

ii. Projection of the future ENSO-TC relationship

Of the four clusters, only NA3 showed a significant difference in ENSO dominance between the projected RCP8.5 and historical climate simulations (Fig. 12c). This cluster encapsulates long recurving TC tracks forming in the deep tropics. It underwent a subtle (but statistically significant) change and became La Niña dominant under the RCP8.5 projection (Fig. 12c), although we do stress that La Niña TCs were considered statistically dominant over El Niño TCs in the observed records for this cluster. Vertical wind shear (Fig. 2d; Fig. 3d) was projected to decrease (increase) during La Niña (El Niño) events, potentially accounting for this change. Other clusters showed no significant changes between the historical and RCP8.5 simulations.

Track density projections for NA3 (Fig. 13c,d) were consistent over both ENSO phases, indicating a poleward shift of TC genesis locations as also found by Murakami and Wang (2010) in a high-resolution model. This poleward shift is likely to alter the mean trajectories of TC tracks, allowing them to recurve earlier and decrease the likelihood of landfall over the North American continent. Track density projections for high latitude TCs (NA2) indicated a potential shift east in genesis position (Fig. 13a). Projected changes in TC activity (Figs 2a and 3a) and in the large-scale conditions (Fig. 2b-e; Fig. 3b-e) were largely consistent between both phases of ENSO over the NA basin.

4. Summary

This study investigated the traditional ENSO-TC track relationship in a selected group of coarse-to-medium resolution CMIP5 models. Models were selected for each TC basin based on their performance in that basin; with between four and seven models used for each basin. A track cluster analysis was applied in each TC basin to produce distinct groups of similar TC tracks. Included in this analysis were TC tracks from the observed records, historically simulated TC tracks from CMIP5 models as well as projected TC tracks from CMIP5 models under the RCP8.5 condition. The relative dominance of each cluster by “El Niño” or “La Niña” or "neither" in the observed record, historical simulation and RCP8.5 projection is summarized in Table 8.

The major findings of this study were as follows:

- The historically simulated ENSO modulation of regional TC track clusters is quite similar to that of the observed ENSO modulation. Only seven regional clusters (out of a total of twenty-eight) were shown to be statistically inconsistent between the historical multi-model means and the observed records. Three of these clusters were located in the WNP basin. Interpretation of some results were complicated by the underestimation of TC counts in some clusters, particularly in the ENP and NA basins.
- When comparing the regional TC track clusters between the RCP8.5 and the historical simulations, eleven clusters and four sub-clusters (highlighted in Table 8) were shown to be significantly different in terms of statistical ENSO dominance. However, we do stress here that changes in statistical significance may not always be an indicator of drastic changes to ENSO-TC relationships. For example, a few of the regional clusters that changed dominance, simply went from "slightly La Niña dominant" to "significantly La Niña dominant" (e.g., E2 and NA3). We also note that no cluster went from significantly "El Niño dominant" to significantly "La Niña dominant", or vice versa.
- Regional clusters that were projected to become La Niña dominant under the RCP8.5 projection were found in the central South Indian Ocean (S2, S3), in the southern Bay of Bengal (NI3) and over straight-moving TCs in the South China Sea (W6-H). La Niña TCs often became dominant due to projected decreases in El Niño TCs, rather than an increase in La Niña TCs. This was mostly the case for the central South Indian Ocean (S2, S3, ~60 – 100°E), the southern Bay of Bengal (NI3) as well as straight-moving TCs in the South China Sea (W6-H).

- Regional clusters that were projected to become El Niño dominant under the RCP8.5 projection were mostly exclusive to the western South Pacific (S7) and central North Pacific (E1). El Niño TCs were projected to increase their dominance over La Niña TCs in a larger area of the western South Pacific (~160°E – 165°W), including that of westward directed TCs in the Coral Sea (S6-West), as well as the central North Pacific Ocean (W8-G and E1, ~160°E – 145°W).
- Three regional clusters were projected to become ENSO-neutral under the RCP8.5 projection (two were El Niño dominant and one was La Niña dominant in the historical simulation). Notably all three were considered ENSO-neutral in the observed records. The two formerly El Niño dominant clusters (W7-D and W9-I) related to straight-moving TCs in the northwest Pacific (near the Philippines and China). The formerly La Niña dominant cluster (S1) was located in the far southwest Indian Ocean (near Madagascar).
- Projections of TC lifetimes for all clusters indicated only one statistically significant change. This was for eastward moving TCs in the Coral Sea (S6-East) during El Niño events, that were projected to have longer lifetimes (~3 days).

As climate models improve further, it is anticipated that more studies will be undertaken that consider the impact of ENSO on TC activity, particularly with respect to different types of El Niño and La Niña “flavours”.

Acknowledgements

This work is supported through funding from the Earth Systems and Climate Change Hub of the Australian Government's National Environmental Science Programme (NESP). We thank Kevin Tory and Harvey Ye for their expertise and for supplying the model data. Samuel Bell was supported by an Australian Government Research Training Program (RTP) Stipend and RTP Fee-Offset Scholarship through Federation University Australia.

Appendices

A. OWZ Detection and tracking

The OWZ detection system consists of six parameters (Table A1): minimum thresholds of OWZ at the 850- and 500 hPa levels, relative humidity (RH) at the 950- and 700 hPa levels, specific humidity (SpH) at the 950 hPa level and a maximum threshold of vertical wind shear (VWS) between 850- and 200 hPa. The OWZ variable is a low deformation vorticity parameter used to identify regions favourable for TC formation at the centre of a semi-closed circulation (i.e. a 'marsupial pouch'; Dunkerton et al. 2009), within the lower- to mid-troposphere. More precisely, it is the product of absolute vorticity and the Okubo-Weiss parameter (Okubo 1970; Weiss 1991) normalised by the vertical components of relative vorticity squared such that:

$$OWZ = sgn(f) \times (\zeta + f) \times \max\left[\frac{\zeta^2 - (E^2 + F^2)}{\zeta^2}, 0\right] \quad (1)$$

where f is the Coriolis parameter, $\zeta = \frac{\partial v}{\partial x} - \frac{\partial u}{\partial y}$ the vertical component of relative vorticity, $E = \frac{\partial u}{\partial x} - \frac{\partial v}{\partial y}$ the stretching deformation, and $F = \frac{\partial v}{\partial x} + \frac{\partial u}{\partial y}$ the shearing deformation.

The OWZ detection and tracking scheme is concisely summarized in five dot points below, with further detail accessible in other studies (Tory et al. 2013a; Bell et al. 2018).

a. Each 1° × 1° grid point is assessed based on the initial threshold values of each OWZ-Detector parameter every 12-hrs.

b. When at least two neighbouring grid points satisfy the initial thresholds of each OWZ-Detector parameter, these points are considered to represent a single circulation at that point in time.

c. The circulations from step (b) are linked through time by estimating their position in relation to the circulation's expected position based on an averaged 4º × 4º steering wind at 700 hPa.

d. Tracks are terminated when no circulation match is found in the next two time-steps within a generous (~350 km) latitude dependent radius.

e. The core thresholds are then applied to each storm track, and if they are satisfied for 48-hrs, a TC is declared.

References

Basher RE, Zheng X (1995) Tropical cyclones in the southwest Pacific: Spatial patterns and relationships to Southern Oscillation and sea surface temperature. *J. Climate*, **8**, 1249–1260.

Bayr T, Latif M, Dommenget D, et al (2018) Mean-state dependence of ENSO atmospheric feedbacks in climate models. *Climate Dyn.*, **50**, 3171–3194.

Bell R, Hodges K, Vidale PL, Strachan J, Roberts M (2014) Simulation of the global ENSO–tropical cyclone teleconnection by a high-resolution coupled general circulation model. *J. Climate*, **27**, 6404–6422, doi:https://doi.org/10.1175/JCLI-D-13-00559.1

Bell SS, Chand SS, Tory KJ, Turville C, (2018) Statistical assessment of the OWZ tropical cyclone tracking scheme in ERA-Interim. *J. Climate*, **31**, 2217–2232.

Bell SS, Chand SS, Tory KJ, Dowdy A. J., Turville C., Ye H (2019a) Projections of Southern Hemisphere Tropical Cyclone Track Density using CMIP5 models. *Climate Dyn.*, **52**, 6065–6079.

Bell SS, Chand SS, Camargo SJ, Tory KJ, Turville C, Ye H (2019b) Eastern North Pacific tropical cyclone activity in historical and future CMIP5 experiments: assessment with a model-independent tracking scheme. *Climate Dyn.,* **53**, 4841–4855 https://doi.org/10.1007/s00382-019-04830-0

Bell SS, Chand SS, Camargo SJ, Tory KJ, Turville C, Ye H (2019c) Western North Pacific tropical cyclone tracks in CMIP5 models: Assessment using a model-independent detection and tracking scheme. *J. Climate,* **32**, 7191–7208.

Bell SS, Chand SS, Tory KJ, Turville C, Ye H (2019d) North Indian tropical cyclone activity in CMIP5 experiments: Statistical assessment of future projections using a model-independent detection and tracking scheme. *Submitted to Int. J. Climatol., March 2019.*

Bellenger H et al (2014) ENSO representation in climate models: from CMIP3 to CMIP5. *Climate Dyn.,* **42**, 7-8. doi:10.1007/s00382-013-1783-z

Bi D, Dix M, Marsland S et al (2012) The ACCESS Coupled Model: Description, Control Climate and Evaluation. *Aust. Meteor. Oceanog. J.*, CMIP5 Special Issue, **63**, 41–64.

Boudreault M, Caron LP, Camargo SJ (2017) Reanalysis of climate influences on Atlantic tropical cyclone activity using cluster analysis. *J. Geophys. Res. Atmos*., **122,** 4258–4280, https://doi.org/10.1002/2016JD026103.

Brown JR, Moise AF, Colman RA (2012) The South Pacific Convergence Zone in CMIP5 simulations of historical and future climate. *Climate Dyn.,* **41***,* 2179–2197*,* doi: 10.1007/s00382-012-1591-x.

Cai W, Borlace S, Lengaigne M et al (2014) Increasing frequency of extreme El Niño events due to greenhouse warming, *Nature Clim. Change*, **4**, 111-116.

Camargo SJ, Sobel AH (2005) Western North Pacific Tropical Cyclone Intensity and ENSO. *J. Climate*, **18**, 2996–3006, https://doi.org/10.1175/JCLI3457.1

Camargo SJ (2013) Global and regional aspects of tropical cyclone activity in the CMIP5 models. *J. Climate*, **26**, 9880–9902, https://doi.org/10.1175/JCLI-D-12-00549.1.

Camargo SJ, Robertson AW, Gaffney SJ, Smith P, Ghil M (2007a) Cluster analysis of typhoon tracks. Part I: General properties. *J. Climate*, **20**, 3635-3653.

Camargo SJ, Robertson AW, Gaffney SJ, Smyth P, Ghil M (2007b) Cluster analysis of typhoon tracks: Part II: Large-scale circulation and ENSO. *J. Climate*, **20**, 3654-3676.

Camargo SJ, Emanuel KA, Sobel AH, (2007c) Use of a genesis potential index to diagnose ENSO effects on tropical cyclone genesis. *J. Climate*, **20**, 4819–4834, https://doi.org/10.1175/JCLI4282.1.

Camargo SJ, Robertson AW, Barnston AG, Ghil M (2008) Clustering of eastern North Pacific tropical cyclone tracks: ENSO and MJO effects. *Geochem. Geophys. Geosyst.,* **9**, Q06V05, doi:10.1029/2007GC001861

Capotondi A, Wittenberg AT, Newman M et al (2015) Understanding ENSO diversity. *Bull. Amer. Meteor. Soc.,* **96**, 921–938, https://doi.org/10.1175/BAMS-D-13-00117.1.

Caron L, Boudreault M, Camargo SJ (2015) On the Variability and Predictability of Eastern Pacific Tropical Cyclone Activity. *J. Climate*, **28**, 9678–9696, https://doi.org/10.1175/JCLI-D-15-0377.1

Chan JCL (1985) Tropical cyclone activity in the northwest Pacific in relation to the El Niño/Southern Oscillation phenomenon. *Monthly Weather Review,* **113**, 599–606.

Chan JCL (2000) Tropical cyclone activity over the western North Pacific associated with El Niño and La Niña events. *J. Climate*, **13**, 2960–2972.

Chand SS, Tory KJ, Ye H, Walsh KJE (2017) Projected increase in El Niño-driven tropical cyclone frequency in the Pacific. *Nature Climate Change,* **7**, 123–127, doi:10.1038/nclimate3181.

Chand SS, McBride JL, Tory KJ, Wheeler MC, Walsh KJE (2013) Impact of different ENSO regimes on southwest Pacific tropical cyclones. *J. Climate*, **26**, 600–608, https://doi.org/10.1175/JCLI-D-12-00114.1.

Chand SS, Walsh KJE (2011) Influence of ENSO on Tropical Cyclone Intensity in the Fiji Region. *J. Climate*, **24**, 4096–4108, https://doi.org/10.1175/2011JCLI4178.1

Chia H, Ropelewski C (2002) The Interannual Variability in the Genesis Location of Tropical Cyclones in the Northwest Pacific. *J. Climate*, **15**, 2934-2944.

Christensen JH et al (2013) Climate phenomena and their relevance for future regional climate change. In: Stocker TF, and Coauthors, eds. *Climate Change 2013: The Physical Science Basis. Contribution of Working Group I to the Fifth Assessment Report of the Intergovernmental Panel on Climate Change* (IPCC AR5). Cambridge, UK and New York, NY: Cambridge University Press.

Chu PS (2004) ENSO and tropical cyclone activity. Hurricanes and Typhoons: Past, Present, and Future, R. J. Murnane and K.-B. Liu, Eds., Columbia University Press, 297–332.

Chu PS, Wang J (1997) Tropical cyclone occurrences in the vicinity of Hawaii: Are the differences between El Niño and non-El Niño years significant? *J. Climate,* **10**, 2683–2689.

Colbert AJ, Soden BJ, Kirtman BP (2015) The impact of natural and anthropogenic climate change on western North Pacific tropical cyclone tracks. *J. Climate*, **28**, 1806–1823.

Collier MA, Jeffrey SJ, Rotstayn LD et al (2011) The CSIRO-Mk3.6.0 Atmosphere-Ocean GCM: participation in CMIP5 and data publication. In: 19th International Congress on Modelling and Simulation, Perth, Australia, 12–16 December 2011 http://mssanz.org.au/modsim2011

Collins JM, Mason IM (2000) Local environmental conditions related to seasonal tropical cyclone activity in the Northeast Pacific basin. *Geophysical Research Letters*, **27**, 3881–2884.

Collins M et al (2010) The impact of global warming on the tropical Pacific Ocean and El Niño. *Nature Geoscience*. **3**, 391-397. 10.1038/ngeo868.

CSIRO and Bureau of Meteorology (2015) Climate Change in Australia (CCiA). Information for Australia's Natural Resource Management Regions. Technical Report, *CSIRO and Bureau of Meteorology*, Australia

Daloz AS, Camargo SJ, Kossin JP et al (2015) Cluster analysis of down-scaled and explicitly simulated North Atlantic tropical cyclone tracks. *J. Climate*, **28**, 1333–1361, doi:0.1175/JCLI-D-13-00646.1.

Daloz AS, Chauvin F, Walsh KJE, Lavender SL, Abbs D, Roux F (2012) The ability of general circulation models to simulate tropical cyclones and their precursors over the North Atlantic main development region. *Climate, Dyn*., **39**, 1559–1576.

Davis CA, (2018) Resolving tropical cyclone intensity in models. *Geophys. Rea. Lett.*, **45**, 2082–2087. https://doi-org.ezproxy.federation.edu.au/10.1002/2017GL076966

Diamond HJ, Lorrey AM, Renwick JA (2013) A Southwest Pacific Tropical Cyclone Climatology and Linkages to the El Niño–Southern Oscillation. *J. Climate,* **26**, 3–

25, https://doi.org/10.1175/JCLI-D-12-00077.1

Donner LJ, Wyman BL, Hemler RS et al (2011) The dynamical core, physical parameterizations, and basic simulation characteristics of the atmospheric component AM3 of the GFDL global coupled model CM3. *J. Climate*, **24**, 3484–3519, doi:10.1175/2011JCLI3955.1.

Dunkerton TJ, Montgomery MT, Wang Z (2009) Tropical cyclogenesis in a tropical wave critical layer: Easterly waves. *Atmos. Chem. Phys*., **9**, 5587–5646.

Emanuel KA (2013) Downscaling CMIP5 climate models shows increased tropical cyclone activity over the 21st century. *Proceedings of the National Academy of Sciences of the United States of America*, **110**, 12,219–12,224, doi:10.1073/pnas.1301293110

Evan AT, Camargo SJ (2011) A Climatology of Arabian Sea Cyclonic Storms. *J. Climate*, 24, 140–158, https://doi.org/10.1175/2010JCLI3611.1

Frank WM, Young GS (2007) The interannual variability of tropical cyclones. *Monthly Weather Review*, **135**, 3587–3598.

Gaffney SJ, Robertson AW, Smyth P, Camargo SJ, Ghil M (2007) Probabilistic clustering of extratropical cyclones using regression mixture models. *Climate Dyn.,* **29**, 423-440.

Gent PR, Danabasoglu G, Donner LJ et al (2011) The community climate system model version 4. *J. Climate Special Collections*, **24,** 4973–4991

Girishkumar MS, Ravichandran M (2012) The influences of ENSO on tropical cyclone activity in the Bay of Bengal during October–December. *J. Geophys. Res.*, **117**, C02033.

Gray WM (1984) Atlantic seasonal hurricane frequency. Part I: El Niño and 30 mb Quasi-Biennial Oscillation influences. *Monthly Weather Review*, **112**, 1649–1668.

Gray WM, Sheaffer JD (1991) El Niño and QBO influences on tropical cyclone activity. In Teleconnections linking worldwide climate anomalies, edited by M. H. Glantz, R. W. Katz, and N. Nicholls, 257–284. New York: Cambridge University Press.

Grose MR, Brown JN, Narsey S, Brown JR, Murphy BF, Langlais C, Gupta AS, Moise AF, Irving DB (2014) Assessment of the CMIP5 global climate model simulations of the western tropical Pacific climate system and comparison to CMIP3. *Int. J. Climatol.,* **34**, 3382–3399. doi:10.1002/joc.3916

Hastings PA (1990) Southern Oscillation influences on tropical cyclone activity in the Australian/South-west Pacific region. *Int. J. Climatol.,* **10**, 291–298.

Held IM, Soden BJ (2006) Robust responses of the hydrologic cycle to global warming. *J. Climate*, **19**, 5686–5699.

Held IM, Zhao M (2011) The response of tropical cyclone statistics to an increase in CO2 with fixed sea surface temperatures. *J. Climate*, **24**, 5353–5364.

Ho C-H, Kim J-H, Jeong J-H, Kim S-H, Chen D-Y (2006) Variation of tropical cyclone activity in the South Indian Ocean: El Niño-Southern Oscillation and Madden-Julian Oscillation effects. *J. Geophys. Rea.,* **111**, doi:0.1029/2006JD007289.

Hong C-C, Li Y-H, Li T et al (2011) Impacts of central Pacific and eastern Pacific El Niños on tropical cyclone tracks over the western North Pacific. *Geophy. Res. Lett.,* **38**, L16712, https://doi.org/10.1029/2011GL048821.

Irwin RP, Davis RE (1999) The relationship between the Southern Oscillation Index and tropical cyclone tracks in the eastern North Pacific. *Geophys. Res. Lett.*, **20**, 2251–2254.

Jien JY, Gough WA, Butler K (2015) The influence of El Niño–Southern Oscillation on tropical cyclone activity in the eastern North Pacific basin. *J. Climate,* **28**, 2459–2474, https://doi.org/10.1175/JCLI-D-14-00248.1.

Jin F-F, Boucharel J, Lin I-I (2014) Eastern Pacific tropical cyclones intensified by El Niño delivery of subsurface ocean heat. *Nature*, **516**, 82–85.

Joint Typhoon Warning Center (2017) JTWC (Joint Typhoon Warning Center) best track dataset. [Available online at https://www.usno.navy.mil/NOOC/nmfc-ph/RSS/jtwc/best_tracks/] Subset used: January 1970–December 2000, accessed 7 September 2017

Jones CD, Hughes JK, Bellouin N et al (2011) The HadGEM2-ES implementation of CMIP5 centennial simulations. *Geosci. Model Dev.,* **4**, 543–570.

Kim H-M, Webster PJ, Curry JA (2011) Modulation of North Pacific tropical cyclone activity by three phases of ENSO. *J. Climate*, **24**, 1839–1849, https://doi.org/10.1175/2010JCLI3939.1.

Kim ST, Yu J-Y (2012) The two types of ENSO in CMIP5 models. *Geophys. Res. Lett.,* **39**, L11704, https://doi.org/10.1029/2012GL052006.

Kimberlain TB (1999) The effects of ENSO on North Pacific and North Atlantic tropical cyclone activity. In Preprints of the 23rd Conference on Hurricanes and Tropical Meteorology, 250–253. Boston: American Meteorological Society.

Knapp KR, Kruk MC, Levinson DH, Diamond HJ, Neumann CJ (2010) The international best track archieve for climate stewardship (IBTrACS) unifying tropical cyclone data. *Bull. Am. Meteor. Soc.*, **91**, 363–376.

Knutti R, Masson D, Gettelman A (2013) Climate model genealogy: Generation CMIP5 and how we got there. *Geophys. Res. Lett.* **40**, 1194–1199.

Kossin JP, Camargo SJ, Sitkowski M (2010) Climate modulation of North Atlantic hurricane tracks. *J. Climate,* **23**, 3057–3076, https://doi.org/10.1175/2010JCLI3497.1.

Kossin JP (2018) A global slowdown of tropical-cyclone translation speed. *Nature*, **558**, 104–107.

Kozar ME, Mann ME, Camargo SJ, Kossin JP, Evans JL (2012) Stratified statistical models of North Atlantic basin-wide and regional tropical cyclone counts, *J. Geophys. Res.*, **117**, D18103, doi:10.1029/2011JD017170.

Kuleshov Y, Ming FC, Qi L, Chouaibou I, Hoareau C, Roux F (2009) Tropical cyclone genesis in the Southern Hemisphere and its relationship with the ENSO. *Ann. Geophys.,* **27,** 2523–2538.

Lavender SL, Dowdy AJ (2016) Tropical cyclone track direction climatology and its intraseasonal variability in the Australian region, *J. Geophys. Res. Atmos.*, **121**, 13,236–13,249, doi:10.1002/2016JD025562.

Lin I-I, Camargo SJ, Patricola C, Boucharel J, Chand SS, Klotzbach PJ, Chan JCL, Wang B, Chang P, Li T, Jin FF (2019) ENSO and tropical cyclones, in ENSO in a changing climate, *AGU Monograph,* submitted December 2018, revised February 2019.

Magee AD, Verdon-Kidd DC, Diamond HJ et al (2017) Influence of ENSO, ENSO Modoki, and the IPO on tropical cyclogenesis: a spatial analysis of the southwest Pacific region. *Int. J. Climatol,* **37,** 1118-1137, doi:10.1002/joc.5070

Martin ER, Thorncroft M (2015) Representation of African Easterly Waves in CMIP5 Models. *J. Climate*, **28**, 7702–7715, https://doi.org/10.1175/JCLI-D-15-0145.1

Murakami H, Wang B (2010) Future Change of North Atlantic Tropical Cyclone Tracks: Projection by a 20-km-Mesh Global Atmospheric Model. *J. Climate*, **23**, 2699–2721, https://doi.org/10.1175/2010JCLI3338.1

Murakami H, Wang B, Li T, Kitoh A (2013) Projected increase in tropical cyclones near Hawaii. *Nat. Climate Change*, **3**, 749–754, https://doi.org/10.1038/nclimate1890.

Murphy BF, Ye H, Delage F (2015) Impacts of variations in the strength and structure of El Niño on Pacific rainfall in CMIP5 models. *Climate Dyn*., **44**, 3171–3186.

Ng EK, Chan JCL (2012) Interannual variations of tropical cyclone activity over the north Indian Ocean. *Int. J. Climatol.*, **32**, 819-830. doi:10.1002/joc.2304

Nicholls N, (1979) A simple air-sea interaction model. *Quart. J. Roy. Meteor. Soc.,* **105**, 93-105.

Okubo A (1970) Horizontal dispersion of floatable particles in the vicinity of velocity singularities such as convergences. *Deep-Sea Res.,* **17**, 445–454.

Paliwal M, Patwardhan A (2013) Identification of clusters in tropical cyclone tracks of north Indian Ocean. *Nat. Hazards*, **68**, 645–656, https://doi.org/10.1007/s11069-013-0641-y.

Patricola CM, Chang P, Saravanan R (2016) Degree of simulated suppression of Atlantic tropical cyclones modulated 1 by flavour of El Niño. *Nat. Geosci*., **9**, 155–160, https://doi.org/10.1038/ngeo2624.

Patricola CM, Camargo SJ, Klotzbach PJ, Saravanan R, Chang P (2018) The influence of ENSO flavors on western North Pacific tropical cyclone activity. *J. Climate,* **31**, 5395–5416, doi: 10.1175/JCLI-D-17-0678.1

Power S, Delage F, Chung C, Kociuba G, Keay K (2013) Robust twenty-first-century projections of El Niño and related precipitation variability. *Nature,* **502**, 541–545.

Ramsay HA, Camargo SJ, Kim D. (2012) Cluster analysis of tropical cyclone tracks in the Southern Hemisphere. *Climate Dyn.,* **39**, 897–917, doi:10.1007/s00382-011-1225-8.

Ramsay HA, Chand SS, Camargo SJ (2018) A Statistical Assessment of Southern Hemisphere Tropical Cyclone Tracks in Climate Models. *J. Climate,* **31**, 10,081–10,104, https://doi.org/10.1175/JCLI-D-18-0377.1

Ren H.□L, Jin F.□F. (2011) Niño indices for two types of ENSO, *Geophys. Res. Lett.,* **38**, L04704, doi:10.1029/2010GL046031.

Riahi K, Rao S, Krey V, Cho C, Chirkov V, Fischer, G, Kindermann G, Nakicenovic N, Rafaj P (2011) RCP 8.5—A scenario of comparatively high greenhouse gas emissions. *Climatic Change,* **109**, 33-57, doi:10.1007/s10584-011-0149-y

Sanderson B, Knutti R, Caldwell P (2015) A Representative Democracy to Reduce Interdependency in a Multimodel Ensemble. *J. Climate*, **28**, 5171–5194

Sharmila S, Walsh KJE (2018) Recent poleward shift of tropical cyclone formation linked to Hadley cell expansion. *Nature Climate Change*, **8**, 730–736.

Singh OP, Khan TMA, Rahman MS (2001), Probable reasons for enhanced cyclogenesis in the Bay of Bengal during July–August of ENSO years, *Global Planet. Change*, **29**, 135–147, doi:10.1016/S0921-8181(00)00090-4.

Strachan JP, Vidale PL, Hodges K, Roberts M, Demory ME (2013) Investigating global tropical cyclone activity with a hierarchy of AGCMs: The role of model resolution. *J. Climate,* **26**, 133–152, https://doi.org/10.1175/JCLI-D-12-00012.1.

Sugi M, Murakami H, Yoshimura J (2012) On the mechanism of tropical cyclone frequency changes due to global warming. *J. Meteor. Soc. Japan*, **90A**, 397–408.

Takahashi K, Montecinos A, Goubanova K, Dewitte B (2011) ENSO regimes: Reinterpreting the canonical and Modoki El Niño, *Geophys. Res. Lett.,* **38**, L10704, doi:10.1029/2011GL047364.

Tan K, Huang P, Liu F, Murakami H, Hsu P (2019) Simulated ENSO's impact on tropical cyclone genesis over the western North Pacific in CMIP5 models and its changes under global warming. *Int J Climatol.* **39**, 3668–3678. https://doi.org/10.1002/joc.6031

Taschetto AS. et al (2014) Cold tongue and warm pool ENSO events in CMIP5: mean state and future projections. *J. Climate*, **27**, 2861–2885.

Taylor KE, Stouffer RJ, Meehl GA (2012) An overview of CMIP5 and the experiment design. Bull. Am. Meteor. Soc. **93**, 485–498.

Tory KJ, Dare RA, Davidson NE, McBride JL, Chand SS (2013a) The importance of low-deformation vorticity in tropical cyclone formation. *Atmos. Chem. Phys*. **13**, 2115–2132.

Tory KJ, Chand SS, Dare RA, McBride JL (2013b) The development and assessment of a model-, grid- and basin independent tropical cyclone detection scheme. *J. Climate,* **26,** 5493–5507.

Tory KJ, Chand SS, McBride JL, Ye H, Dare RA (2013c) Projected changes in late 21st century tropical cyclone frequency in thirteen coupled climate models from the coupled model intercomparison project phase 5. *J Climate,* **26**, 9946–9959.

Tory KJ, Dare RA (2015) Sea surface temperature thresholds for tropical cyclone formation. *J Climate*, **28**, 8171–8183

Tory KJ, Ye H (2018) Projected Changes of Tropical Cyclone Formation Regions in the Southern Hemisphere. In: 33rd Conference on Hurricanes and Tropical Meteorology, 16 – 20 April 2018. American Meteorological Society, Ponte Vedra, FL.

Trenberth KE, (1997) The definition of El Niño. *Bull Amer. Meteor. Soc.,* **78**, 2771–2778.

Vecchi GA, Soden BJ (2007) Global warming and the weakening of the tropical circulation. *J. Climate*, **20,** 4316–4340.

Voldoire A, Sanchez-Gomez E, Salas y Mélia D et al (2012) The CNRM-CM5.1 global climate model: description and basic evaluation. *Climate Dyn.,* **40**, 2091–2121.

Wahiduzzaman M, Oliver E, Wotherspoon SJ, Holbrook NJ (2017) A climatological model of North Indian Ocean tropical cyclone genesis, tracks and landfall. *Climate Dyn*., doi:10.1007/s00382-016-3461-4.

Walsh KJE, Camargo SJ, Vecchi GA et al (2015) Hurricanes and climate: the U.S.

CLIVAR working group on hurricanes. *Bull. Amer. Meteorol. Soc.* **96**, 997-1017.

Wang C, Wu L (2015) Influence of future tropical cyclone track changes on their basin-wide intensity over the western North Pacific: Downscaled CMIP5 projections. *Adv. Atmos. Sci.* **32**, 613–623.

Watanabe M, Suzuki T, O'ishi R et al (2010) Improved climate simulation by MIROC5: Mean states, variability, and climate sensitivity. *J. Climate*, **23**, 6312–6335, doi:10.1175/2010JCLI3679.1.

Weiss J (1991) The dynamics of enstrophy transfer in two-dimensional hydrodynamics. *Phys. D*, **48**, 273–294.

Whitney LD, Hobgood JS (1997) The relationship between sea surface temperatures and maximum intensities of tropical cyclones in the eastern North Pacific Ocean. *J. Climate,* **10**, 2921–2930, https://doi.org/10.1175/1520-0442(1997)010,2921:TRBSST.2.0.CO;2.

Wu L, Zhang H, Chen J-M et al (2018) Impact of Two Types of El Niño on Tropical Cyclones over the Western North Pacific: Sensitivity to Location and Intensity of Pacific Warming. *J. Climate*, **31**, 1725-1742.

Wu T, Song L, Weiping L et al (2014) An overview of BCC climate system model development and application for climate change studies. *J. Meteor. Res.*, **28,** 34–56, doi:10.1007/s13351-014-3041-7.

Yeh S-W, Kug J-S, Dewitte B, Kwon M-H, Kirtman BP, Jin F-F, (2009) El Niño in a changing climate. *Nature*, **461**, 511–514, https://doi.org/10.1038/nature08316.

Ying M, Cha E-J, Kwon HJ (2011) Comparison of three western North Pacific tropical cyclone best track datasets in a seasonal context. *J. Meteor. Soc. Japan*, **89**, 211–224, http://doi.org/10.2151/jmsj.2011-303.

Zhang W, Vecchi GA, Murakami H, Delworth T, Wittenberg AT, Rosati A, Underwood S, Anderson W, Harris L, Gudgel R, Lin S, Villarini G, Chen J, (2016a) Improved Simulation of Tropical Cyclone Responses to ENSO in the Western North Pacific in the High-Resolution GFDL HiFLOR Coupled Climate Model. *J. Climate*, **29**, 1391–1415, https://doi.org/10.1175/JCLI-D-15-0475.1

Zhang W, Vecchi GA, Villarini G, Murakami H, Delworth T, Jia L, Gudgel R, Zemg F (2016b) Simulated Connections between ENSO and Tropical Cyclones near Guam in a High-Resolution GFDL Coupled Climate Model: Implications for Seasonal Forecasting. *J. Climate*, **29**, 8231–8248, https://doi.org/10.1175/JCLI-D-16-0126.1

Figure

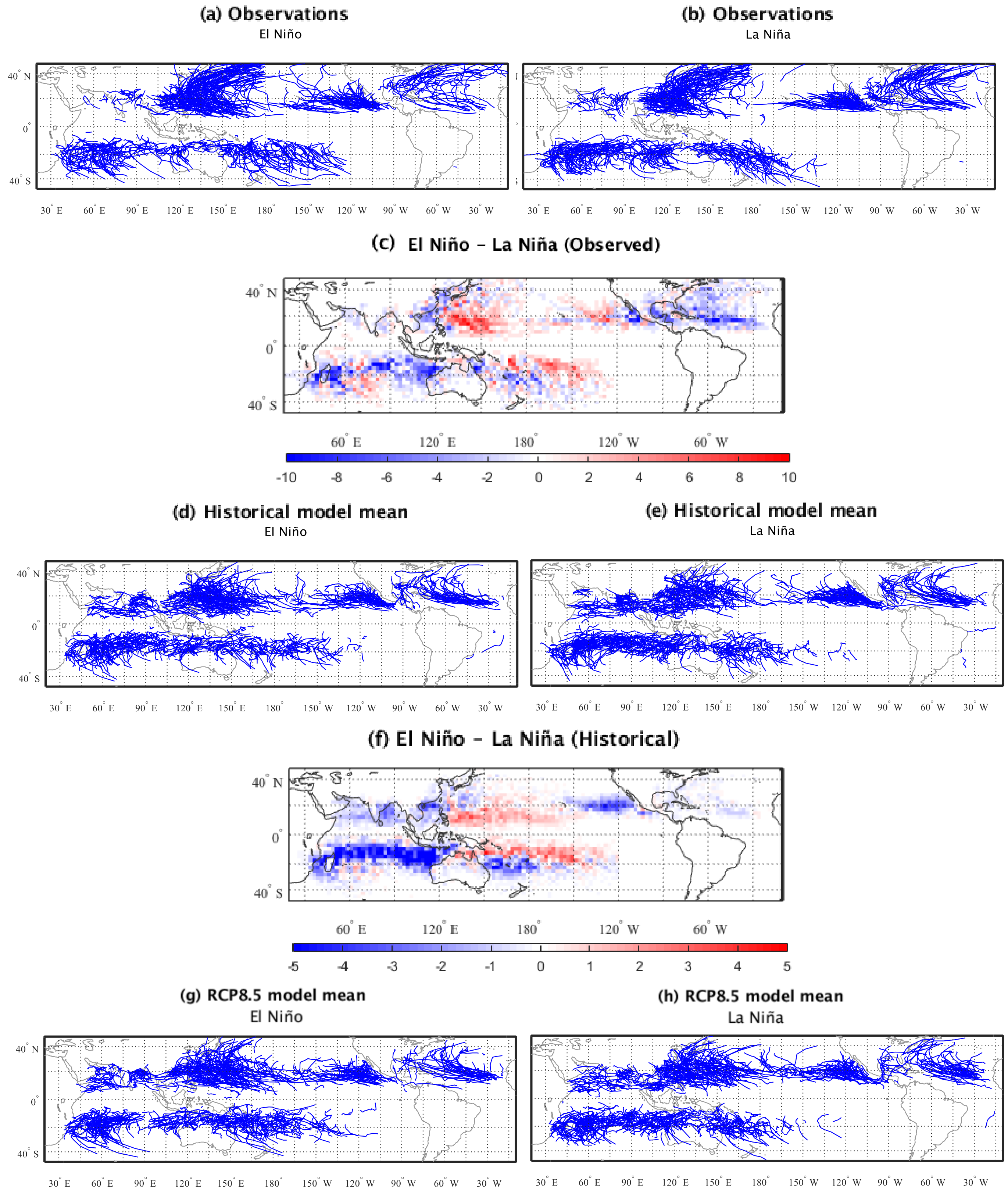

Fig. 1 (a-b, d-e, g-h) Tropical cyclone tracks stratified by ENSO phase as they appear in observations and model simulations. A random selection of tracks, approximately the same in number, from each set of data are displayed (see Tables 1 and 2). The historical model mean displays tracks over the period 1970-2000, while the RCP8.5 model mean displays tracks over the period 2070-2100. In (c) and (f), differences in track density (per decade) are shown, with red (blue) grid boxes indicating a dominance of El Niño (La Niña) tracks.

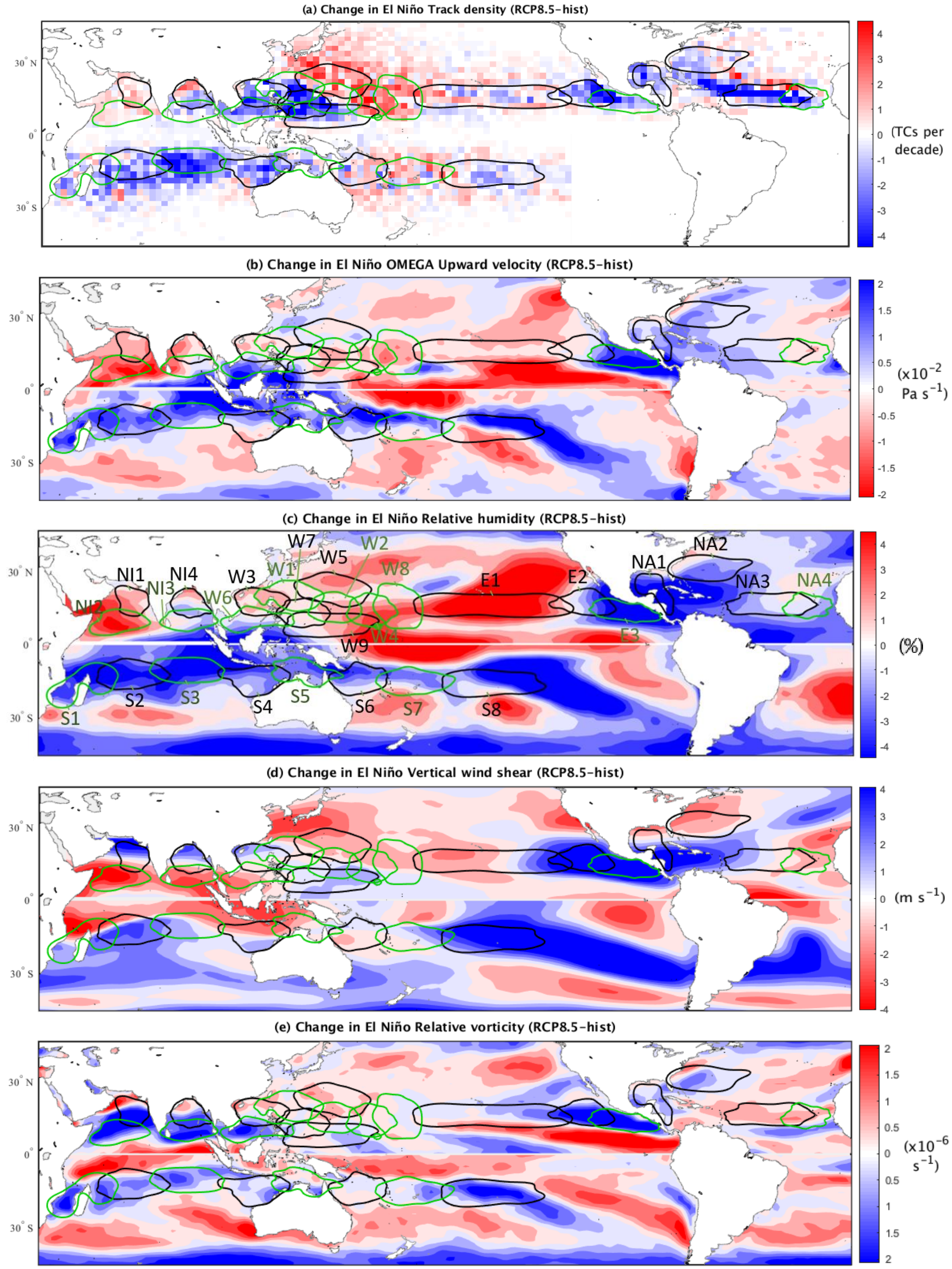

(a) Change in El Niño Track density (RCP8.5-hist)
(TCs per decade)
(b) Change in El Niño OMEGA Upward velocity (RCP8.5-hist)
(x10^{-2} Pa s^{-1})
(c) Change in El Niño Relative humidity (RCP8.5-hist)
(%)
NI1
NI2
NI3
NI4
W1
W2
W3
W4
W5
W6
W7
W8
W9
E1
E2
E3
NA1
NA2
NA3
NA4
S1
S2
S3
S4
S5
S6
S7
S8
(d) Change in El Niño Vertical wind shear (RCP8.5-hist)
(m s^{-1})
(e) Change in El Niño Relative vorticity (RCP8.5-hist)
(x10^{-6} s^{-1})
30° N
0°
30° S

Fig. 2 Difference in El Niño (a) decadal track density normalised by the number of El Nino events and (b-e) large-scale environmental parameters between RCP8.5 and historical CMIP5 simulations. Red shading indicates a projected increase in (a) track density and (b-e) in the favourability of large-scale environmental TC genesis conditions. Track density in the North Atlantic was normalised by observed TC frequency. Kernel function density estimates enclose approximately 75% of TC genesis in each cluster, appearing as green and black contours. Names of clusters are labelled in Fig. 2c.

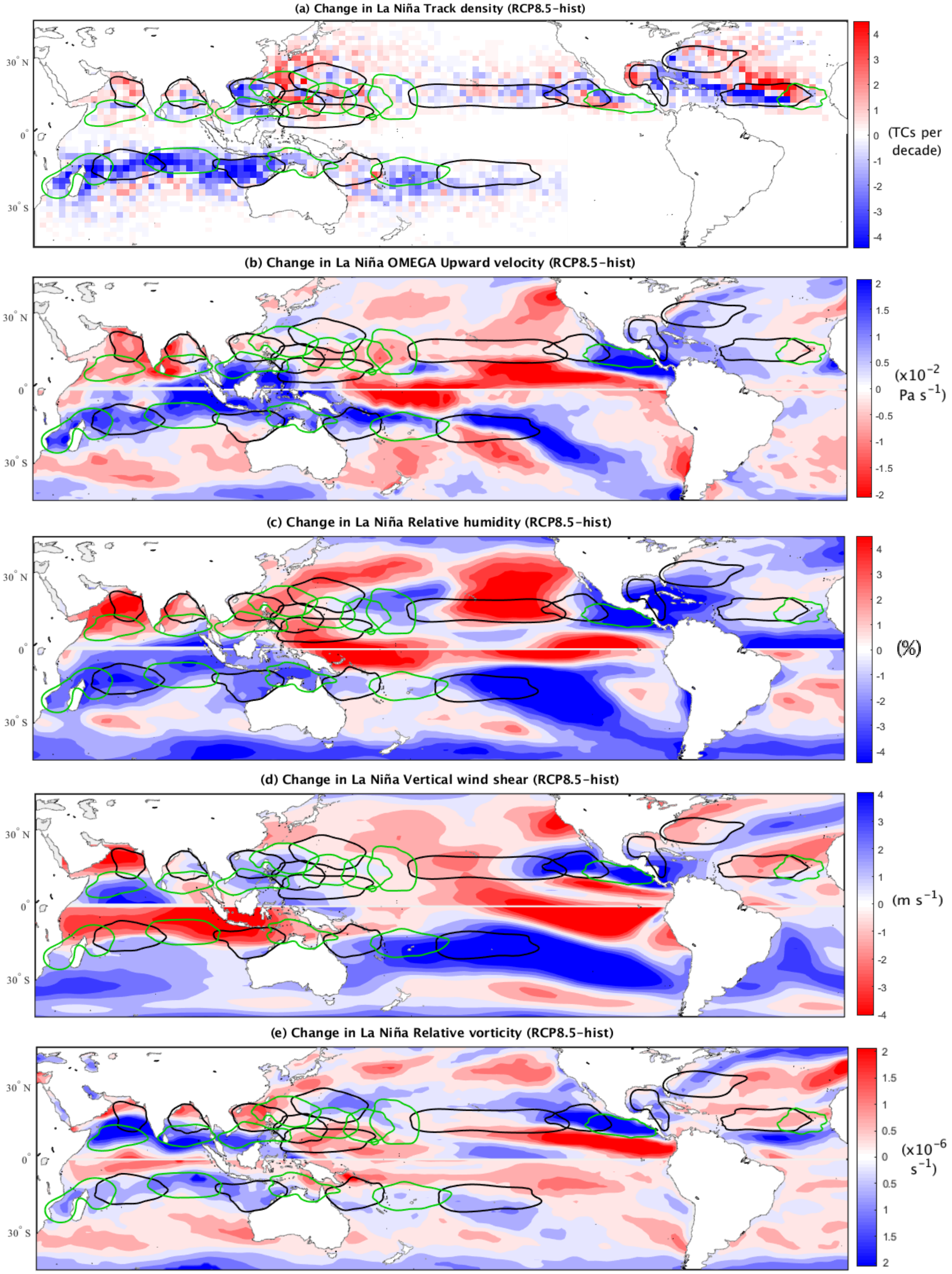
(a) Change in La Niña Track density (RCP8.5-hist)
(TCs per decade)
(b) Change in La Niña OMEGA Upward velocity (RCP8.5-hist)
(x10^{-2} Pa s^{-1})
(c) Change in La Niña Relative humidity (RCP8.5-hist)
(%)
(d) Change in La Niña Vertical wind shear (RCP8.5-hist)
(m s^{-1})
(e) Change in La Niña Relative vorticity (RCP8.5-hist)
(x10^{-6} s^{-1})
30° N
0°
30° S

Fig. 3 As in Fig. 2, but for La Niña.

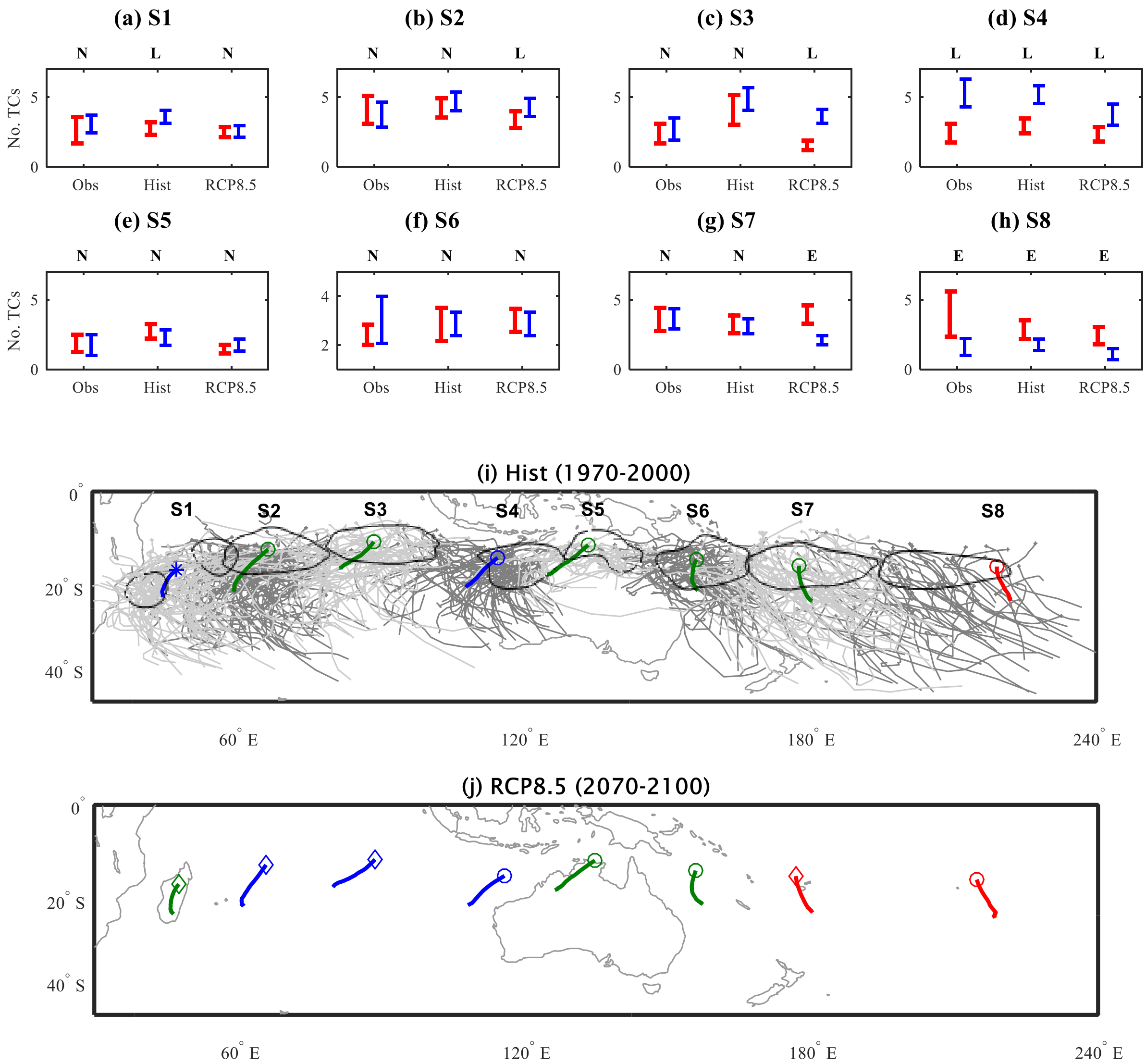

Fig 4 (a-h) The 95% bootstrap confidence intervals (resampled 5000 times) of the number of TCs occurring in El Niño years (red) and La Niña years (blue). Above each plot, a letter (E= El Niño, N=Neither phase dominant or L=La Niña) indicates the statistically dominant phase for that cluster and dataset (Obs=Observations, Hist= multi-model CMIP5 mean 1970-2000, RCP8.5= multi-model CMIP5 mean 2070-2100). A La Niña or El Niño phase is considered dominant when determined to be statistically different under the U-test with 90% confidence using 10,000 mean resamples (bootstrapping) or a 95% confidence interval that does not overlap. (i) Mean cluster trajectories where color indicates phase dominance: El Niño (red), La Niña (blue), or neither phase (green). An inconsistency between observed and historical ENSO dominance is indicated by an asterisk (*). Observed tracks are shown in greyscale, with different shades emphasizing the different clusters. (j) Changes between historical and RCP8.5 phase cluster dominance are indicated by a diamond (◊). Circles (○) indicate correctly simulated ENSO dominance in (i) and no projected change in ENSO dominance in (j).

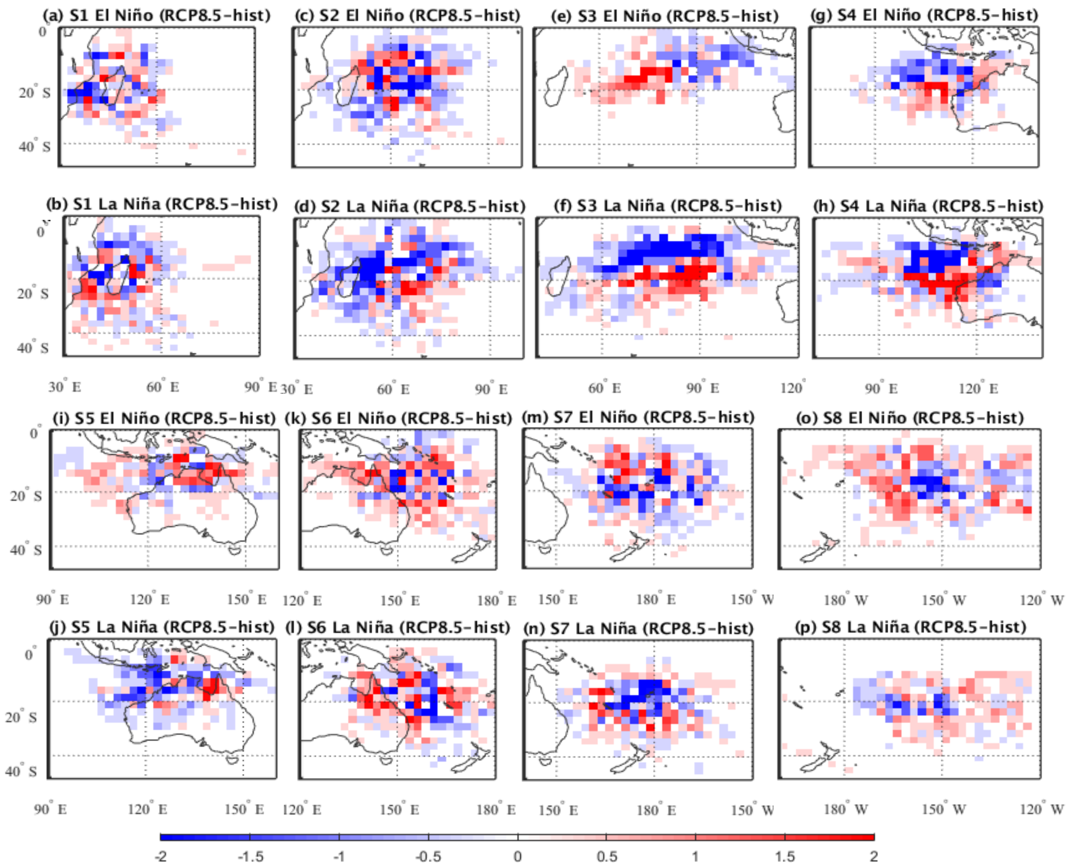

Fig. 5 Difference in cluster TC track densities (per decade) stratified by ENSO with a normalized number of TCs in each cluster, red grid boxes indicate a projected increase in TC track density under RCP8.5.

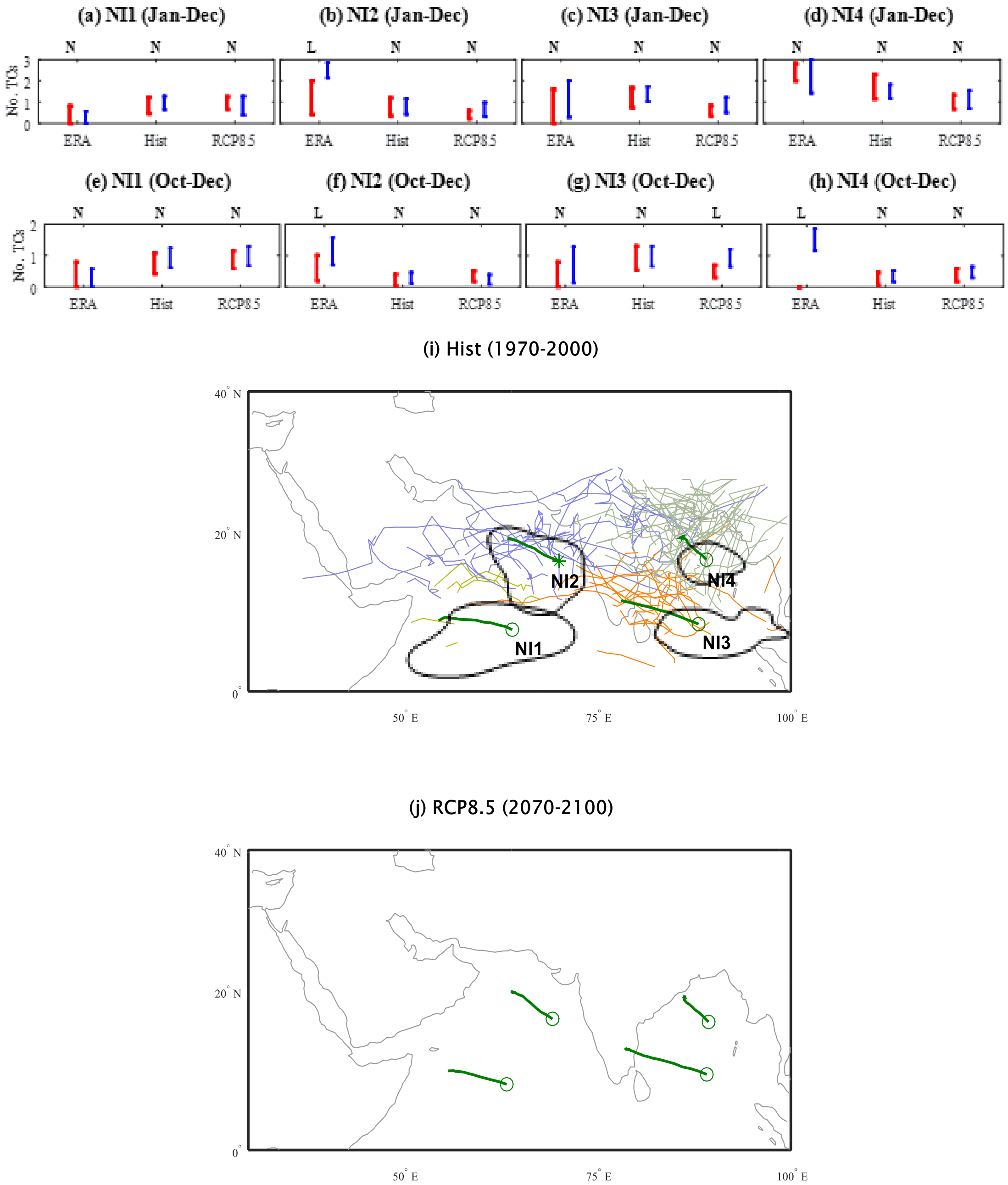

Fig. 6: As in Fig. 4 but for the North Indian region. TCs detected in ERA-Interim (1989-2013, ERA) reanalysis serve as the observations.

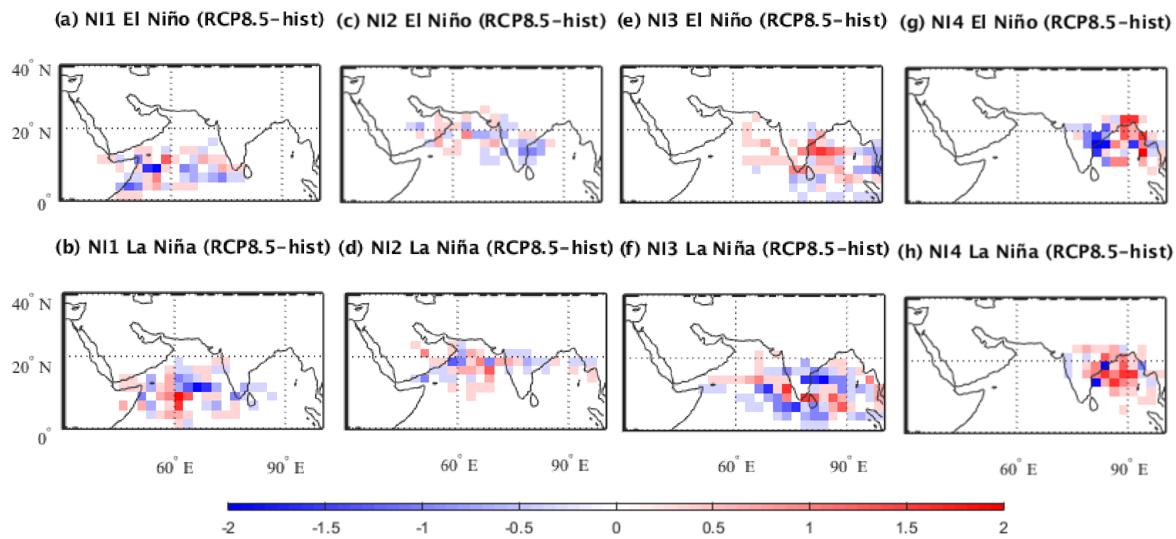

Fig. 7 As in Fig. 5, but for the North Indian clusters.

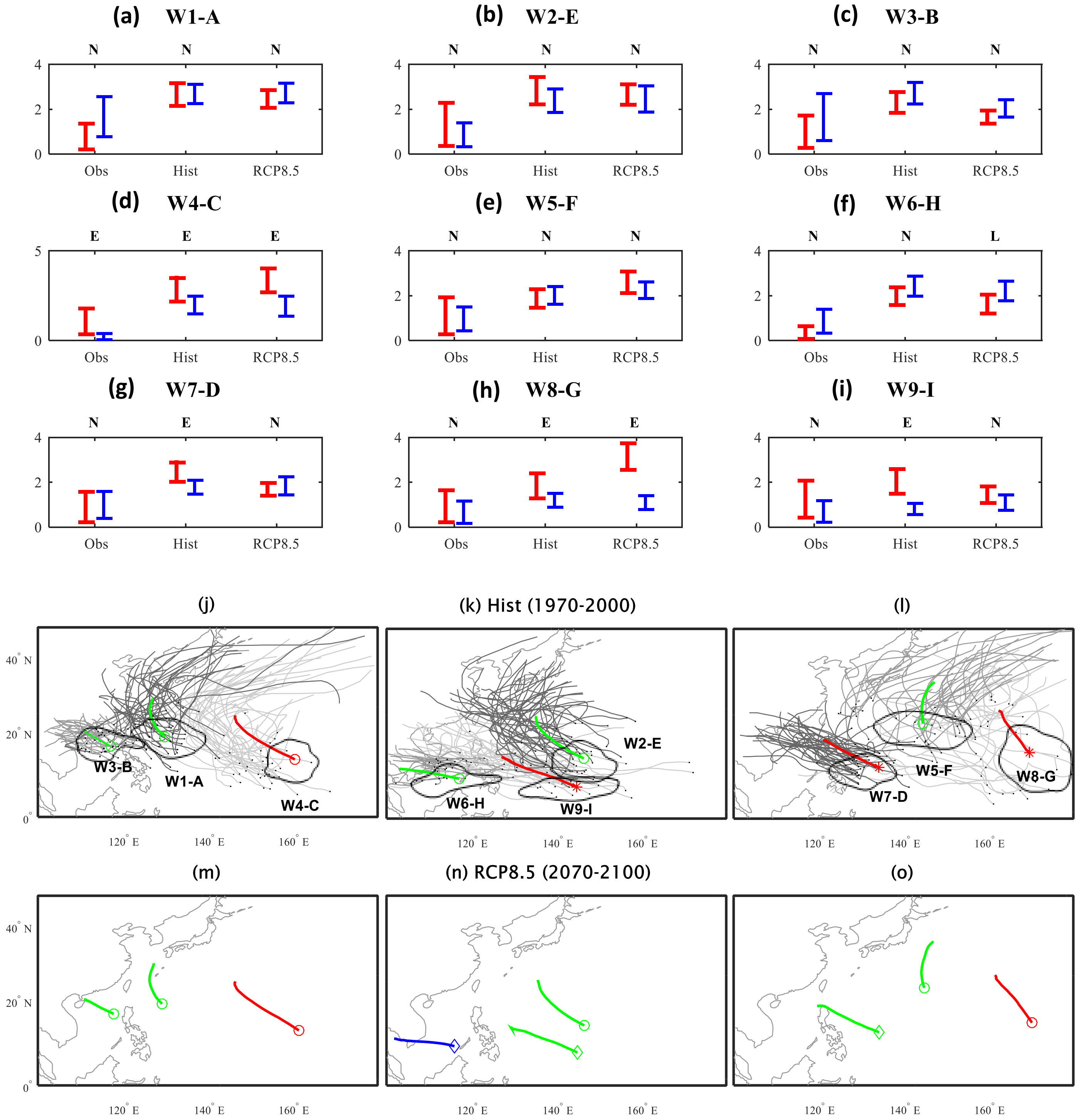

Fig. 8: As in Fig. 4 but for the Western North Pacific.

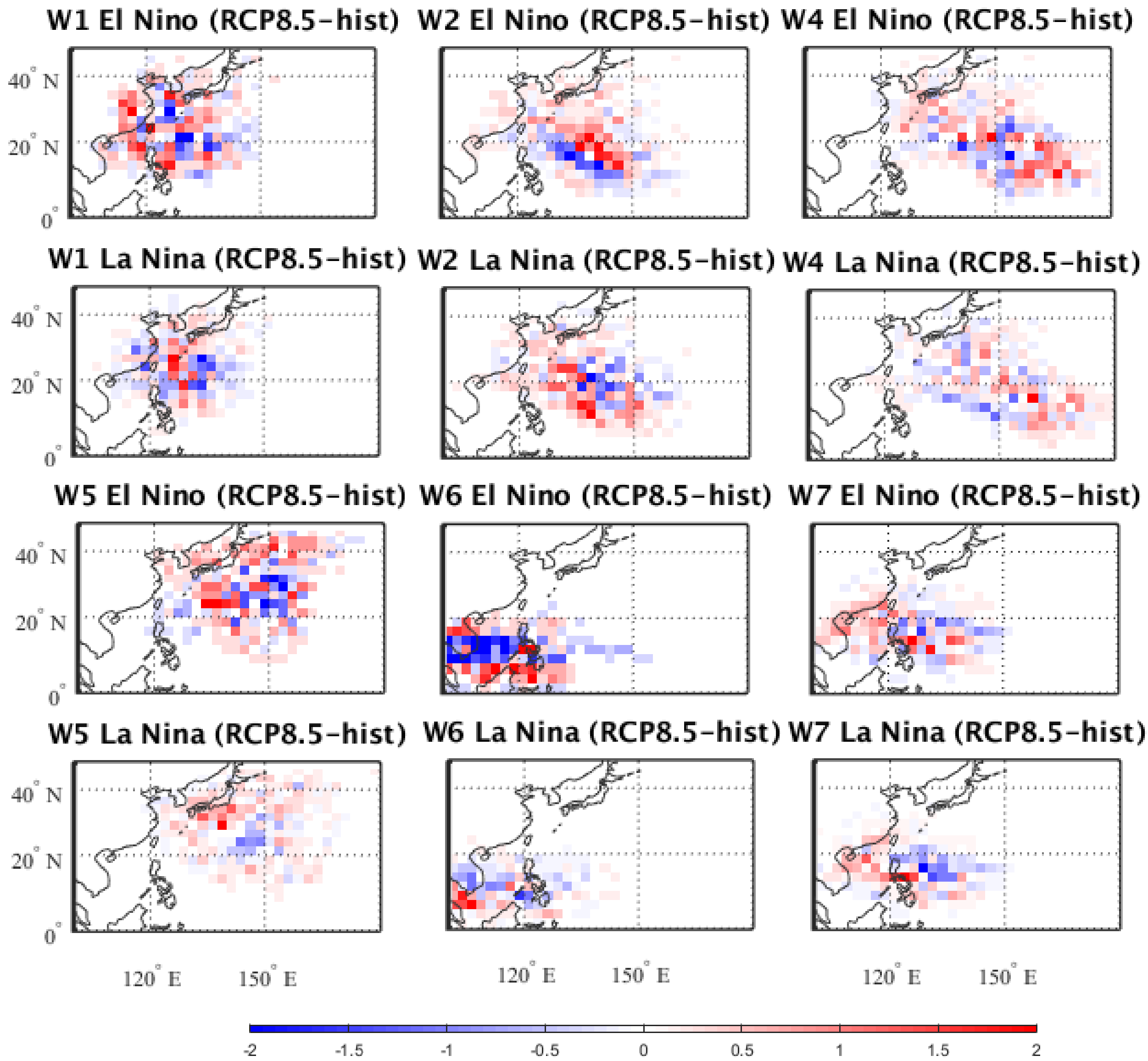

Fig. 9: Difference in TC track density (color bar reads as number of TCs per decade) between RCP8.5 and historical climate with a normalized number of TCs for several WNP clusters (W3, W8 and W9 indicated no clear pattern of change, not shown).

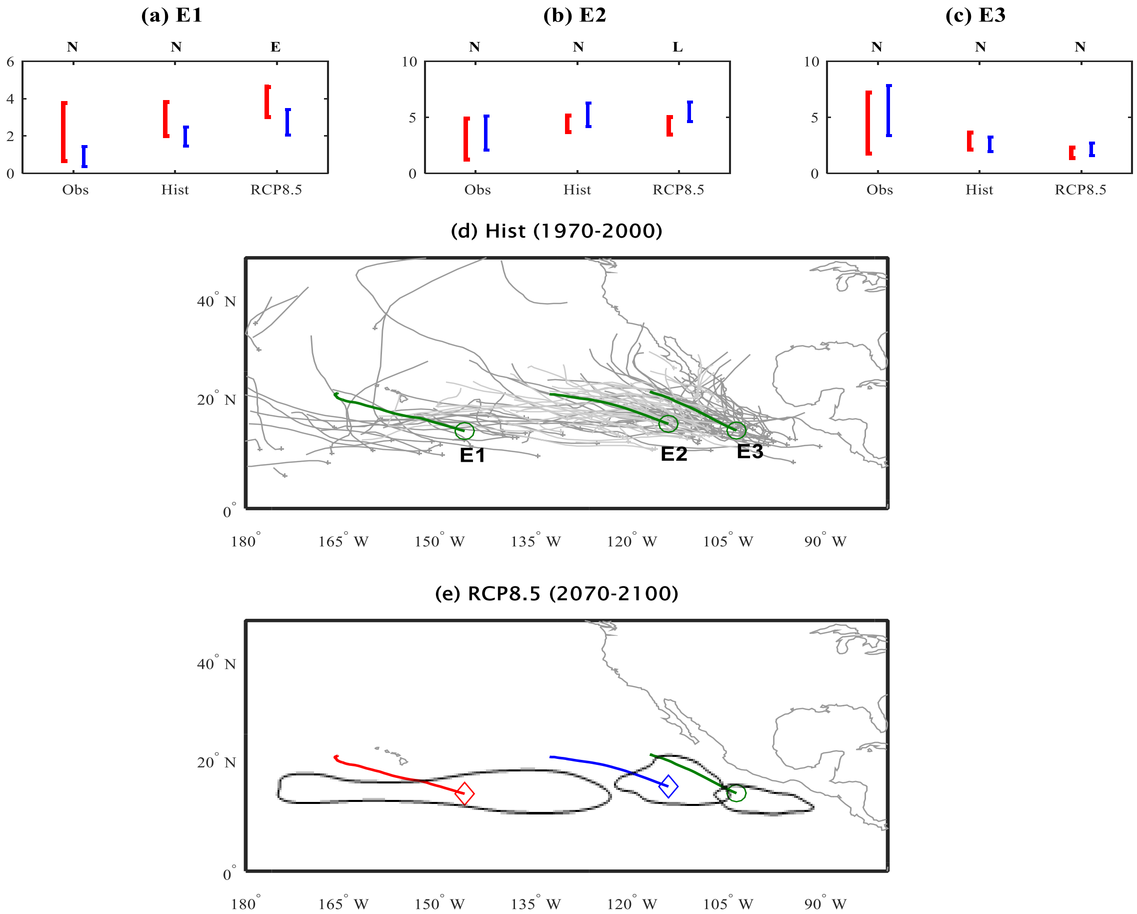

Fig. 10: As in Fig. 4 but for the Eastern North Pacific.

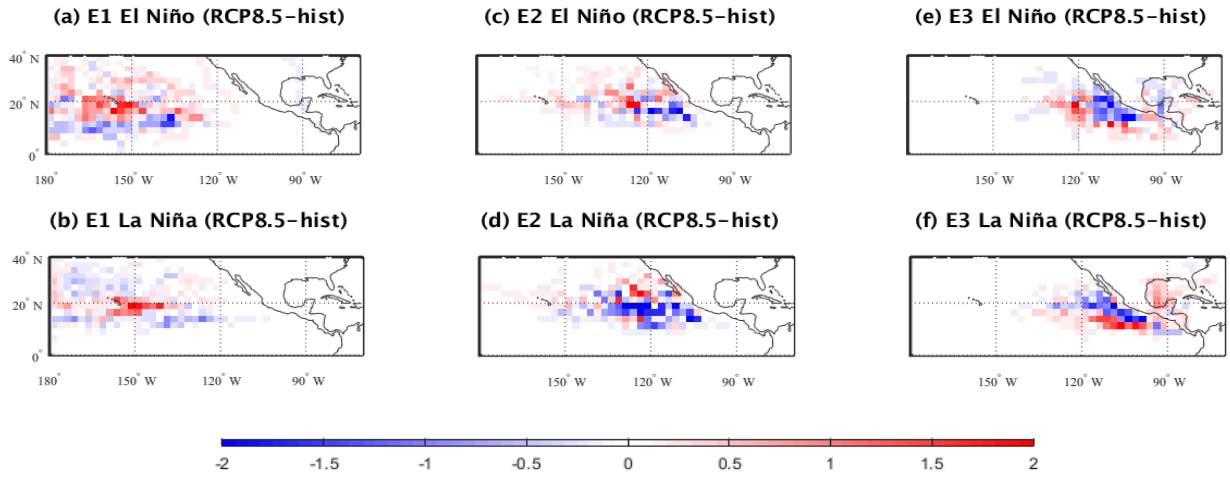

Fig. 11 Difference in TC track density between RCP8.5 and historical climate with a normalized number of TCs for clusters E1-E3 (color bar reads as number of TCs per decade).

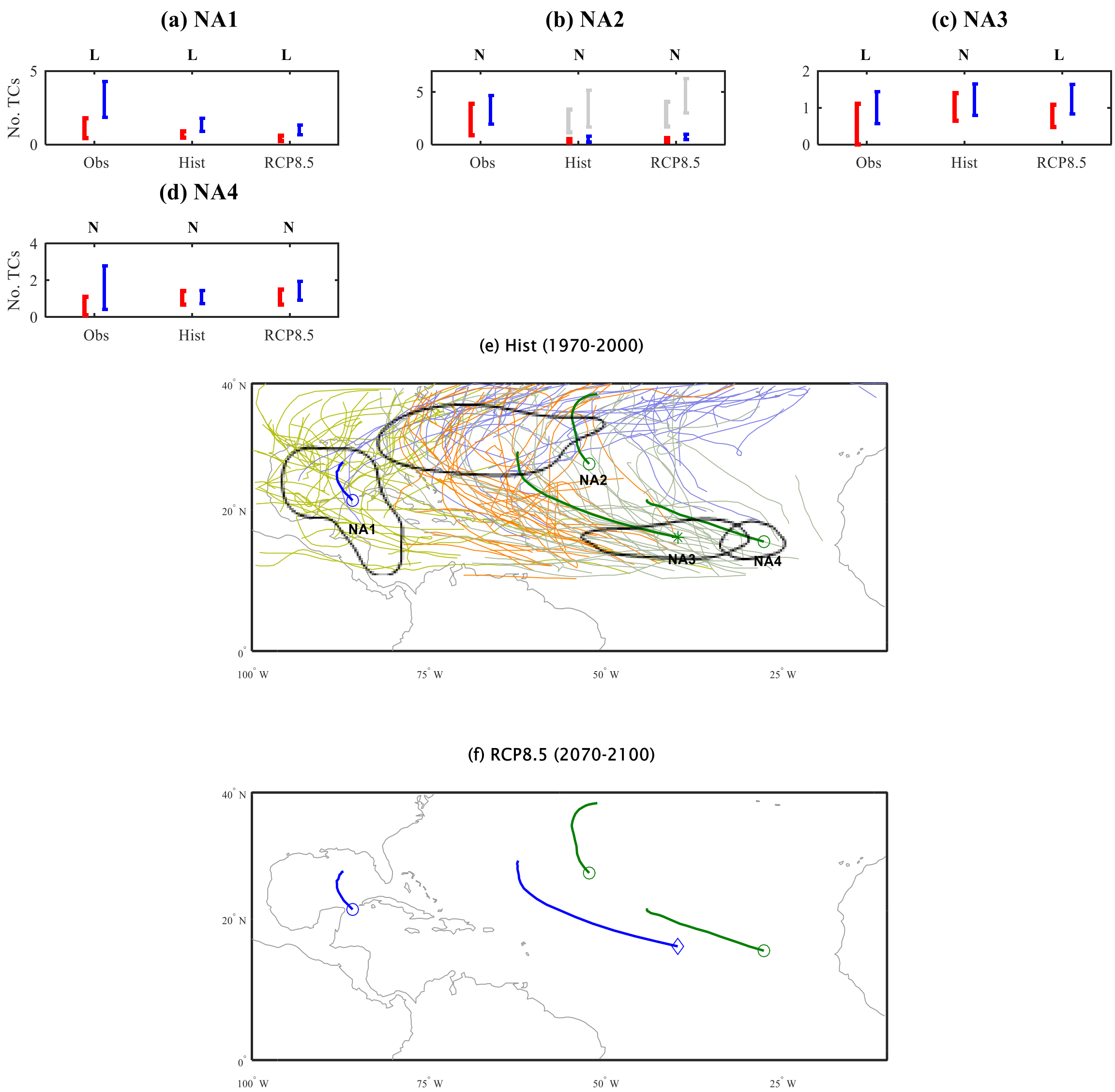

Fig. 12: As in Fig. 4 but for the North Atlantic. Large underestimations of TC numbers in cluster NA2 makes comparison difficult. For this case, bias-corrected TC confidence intervals with respect to observations (grey) were added.

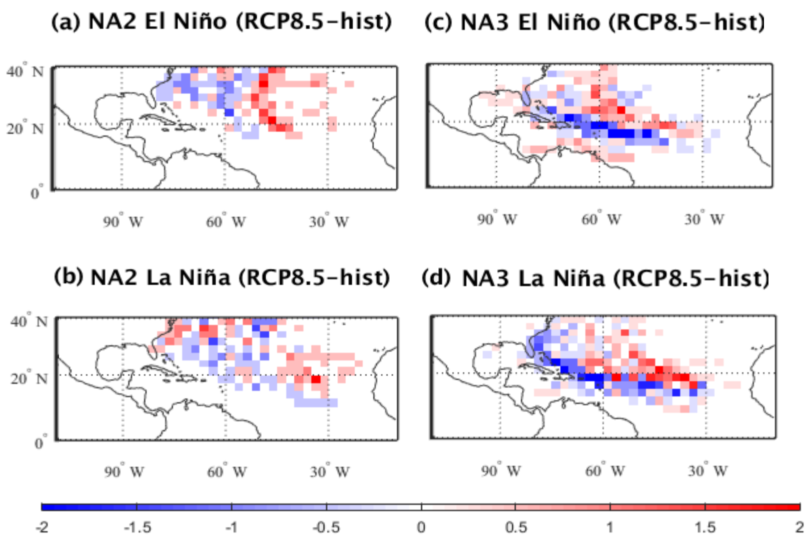

Fig. 13: Difference in TC track density between RCP8.5 and historical climate with a normalized number of TCs for the NA2 and NA3 clusters (color bar reads as number of TCs per decade).

Tables

Table 1: The observational data used in each study region: Southern Hemisphere (SH), North Indian (NI), Western North Pacific (WNP), Eastern North Pacific (ENP) and North Atlantic (NA). *Data preceding 1979 was not cut-off by the subtropical jet.

Region	Observed data	Period
SH (20°E – 120°W)	IBTrACS-WMO	1980/81 to 2015/16
NI (30 – 100°E)	ERA-Interim	1989 to 2013
WNP (100 – 180°E)	JTWC	1970* to 2000
ENP (180 – ~70°W)	IBTrACS-WMO	1970* to 2000
NA (~70°W – 0°)	IBTrACS-WMO	1970* to 2000

Table 2: The twelve CMIP5 models used to form multi-model means for each study region: Southern Hemisphere (SH), North Indian (NI), Western North Pacific (WNP), Eastern North Pacific (ENP) and North Atlantic (NA).

Model	**Horizontal Resolution**	**Region used**	**Basic Description and Reference**
GFDL-ESM2M	*2.5°*		Models developed by the Geophysical Fluid Dynamics Laboratory (GFDL) (Donner et al. 2011)
GFDL-CM3	2.5°	NA	
GFDL-ESM2G	2.5°	NI, WNP, ENP	
ACCESS1.0	1.9°	SH	Developed by the Bureau of Meteorology (BoM) the Australian Community Climate and Earth-System Simulator (ACCESS) models are based on the UK Met Office's Unified Model.(Bi et al. 2012)
ACCESS1.3	1.9°	WNP, NI	
HadGEM2-ES	1.9°	ENP, NA	HadGEM2-ES is a configuration of the UK Met Office's Unified Model.(Jones et al. 2011)
BCC-CSM1.1	2.8°	ENP	Developed by the Beijing Climate Centre (BCC), these models are based on NCAR CCSM2.0.1.(Wu et al. 2014)
BCC-CSM1.1M	1.1°	SH, WNP, NI,	
CSIRO-Mk3.6	1.9°	SH, NI, WNP, ENP, NA	Developed by the Commonwealth Scientific and Industrial Research Organization (CSIRO)(Collier et al. 2011)
CNRM-CM5	1.4°	WNP, ENP, NA	Developed by the Centre National de Recherches Météorologiques (CNRM) (Voldoire et al. 2012)
CCSM4	1.2°	SH, WNP, NI,	Developed by the National Center for Atmospheric Research (NCAR)(Gent et al. 2011)
MIROC5	1.4°	SH, WNP, ENP, NA	Developed by the Model of Interdisciplinary Research on Climate (MIROC) (Watanabe et al. 2010)

Table 3: The choice of the number of clusters, *k*, used in each study region.

Region	No. of clusters (k)	Reference
SH	8	Ramsay et al. (2018); Bell et al. (2019a)
NI	4	Bell et al. (2019d)
WNP	9	Bell et al. (2019c)
ENP	3	Camargo et al. (2008); Bell et al. (2019b)
NA	4	Kossin et al. (2010)

Table 4: Percentage of westward directed TC tracks in each Southern Hemisphere cluster during El Niño and La Niña events. For example, during El Niño events in cluster S1, 63% of TCs in the observed records (obs) tracked westward, 67% of TCs historically simulated by the models (hist) tracked westward and 64% of TCs under the RCP8.5 projection tracked westward. The "Change" column represents the percentage shift toward either east (E) or west (W) from the historical simulation to the RCP8.5 projection. Tracks were defined as "eastward" or "westward" based on their longitude location at two-thirds of their lifetime in relation to genesis.

	El Niño				La Niña			
Cluster	Obs	Hist	RCP8.5	Change	Obs	Hist	RCP8.5	Change
S1	63%	67%	64%	+3%E	73%	72%	60%	+12%E
S2	65%	76%	74%	+2%E	89%	81%	72%	+9%E
S3	59%	62%	71%	+9%W	66%	72%	73%	+1%W
S4	52%	73%	87%	+14%W	64%	75%	83%	+8%W
S5	57%	74%	80%	+6%W	50%	79%	87%	+8%W
S6	57%	52%	62%	+10%W	34%	52%	50%	+2%E
S7	35%	42%	48%	+6%W	12%	45%	47%	+2%W
S8	15%	47%	37%	+10%E	45%	43%	51%	+8%W

Table 5: U-test statistics indicating dominance of either El Niño (positive U-statistic) or La Niña (negative U-statistic), for chosen sub-clusters in the Southern Hemisphere. U-statistics in bold indicate that it exists outside of a 90% confidence interval, in addition an E or L further signifies either El Nino or La Nina dominance.

Cluster	Obs	Hist	RCP8.5
S3-West	-0.89	**-2.09L**	**-3.83L**
S3-East	-0.03	0.43	**-2.36L**
S4-West	**-3.56L**	**-4.38L**	**-2.03L**
S4-East	**-2.21L**	**-1.56L**	**-1.57L**
S5-West	0.73	0.77	-1.12
S5-East	0.09	1.40	0.86
S6-West	0.78	-0.17	**1.54E**
S6-East	-1.21	-0.01	-1.16
S7-West	**2.30E**	-0.06	**3.11E**
S7-East	1.34	0.59	**2.81E**

Table 6: Mean TC Lifetimes (days) for the Southern Hemisphere cluster observations (obs), historical multi-model means (Hist), and projected multi-model means (RCP8.5). Projected changes under RCP8.5 (P_{Change}) indicates either larger (+L) or shorter (+S) lifetimes, bolding represents a significant (95%) change using 5000 bootstrap resamples.

	El Niño				La Niña			
Cluster	Obs	Hist	RCP8.5	P_{Change}	Obs	Hist	RCP8.5	P_{Change}
S1	6.1	5.6	5.1	ΔS	7.7	5.8	6.1	ΔL
S2	8.0	7.5	6.9	ΔS	8.4	7.8	7.0	ΔS
S3-West	8.3	6.9	6.8	ΔS	8.1	8.2	7.0	ΔS
S3-East	8.5	6.2	6.7	ΔL	7.5	6.3	6.3	-
S4-West	4.1	5.3	5.5	ΔL	6.0	5.7	5.5	ΔS
S4-East	5.8	4.5	4.0	ΔS	6.5	5.7	5.7	-
S5-West	5.1	8.8	9.1	ΔL	4.2	7.2	6.9	ΔS
S5-East	5.6	6.8	8.3	ΔL	5.0	8.0	5.6	ΔS
S6-West	8.1	7.8	7.9	ΔL	5.5	6.1	6.4	ΔL
S6-East	7.6	**6.2**	**9.1**	**ΔL**	5.2	6.2	7.2	ΔL
S7	7.1	6.1	5.6	ΔS	5.2	5.2	5.0	ΔS
S8	4.7	4.9	5.8	ΔL	4.9	5.0	5.1	ΔS

Table 7: Mean TC lifetimes (days) for Northern Hemisphere track cluster historical multi-model mean (Hist), and projected multi-model mean (RCP8.5). Projected changes under RCP8.5 (P_{Change}) indicates either larger (+L) or shorter (+S) lifetimes, bolding represents a significant (95%) change using 5000 bootstrap resamples.

	El Niño			La Niña		
Cluster	Hist	RCP8.5	P_{Change}	Hist	RCP8.5	P_{Change}
NI1	5.6	4.7	ΔS	5.4	5.7	ΔL
NI2	6.7	5.0	ΔS	4.7	5.6	ΔL
NI3	5.0	5.8	ΔL	5.7	6.0	ΔL
NI4	5.4	5.2	ΔS	4.8	5.3	ΔL
W1-A	5.5	5.8	ΔL	5.5	5.4	ΔS
W2-E	6.9	6.9	-	6.6	7.1	ΔL
W3-B	5.7	5.9	ΔL	5.2	4.9	ΔL
W4-C	7.1	7.4	ΔL	6.9	6.8	ΔS
W5-F	4.6	4.9	ΔL	4.2	4.8	ΔL
W6-H	7.6	6.7	ΔS	6.9	6.5	ΔS
W7-D	6.7	7.2	ΔL	6.6	7.2	ΔL
W8-G	6.7	7.4	ΔL	5.8	5.8	-
W9-I	10.2	9.5	-	10.1	9.7	ΔS
E1	5.6	5.9	ΔL	4.9	5.5	ΔL
E2	4.9	5.1	ΔL	5.7	5.5	ΔS
E3	6.0	6.3	ΔL	5.9	6.5	ΔL
NA1	4.5	4.4	ΔS	4.7	5.6	ΔL
NA2	4.1	5.0	ΔL	6.2	5.3	ΔS
NA3	6.6	6.6	-	6.6	6.0	ΔS
NA4	5.4	5.6	ΔL		5.0	5.0

Table 8: Summary of the statistical dominance of ENSO in each cluster, including sub-clusters in the Southern Hemisphere, where E represents “El Niño dominant”, L represents “La Niña dominant” and N represents “neither phase”. The likely mechanisms (LM) responsible for changes in model ENSO dominance: relative humidity (RH), vertical wind shear (WS), omega (OM) or relative vorticity (RV). Note that the NI results displayed are over the post-monsoon period. Change of ENSO dominance between model simulations are highlighted in bold.

Southern Hemisphere				**LM**	**Northern Hemisphere**				**LM**
Cluster	Obs	Hist	RCP8.5		**Cluster**	Obs	Hist	RCP8.5	
S1	N	**L**	**N**		**NI1**	N	N	N	
S2	N	**N**	**L**		**NI2**	L	N	N	
S3 (Overall)	N	**N**	**L**	RH; WS	**NI3**	N	**N**	**L**	
West	N	L	L		**NI4**	L	N	N	
East	N	**N**	**L**		**W1-A**	N	N	N	
S4 (Overall)	L	L	L		**W2-E**	N	N	N	
West	L	L	L		**W3-B**	N	N	N	
East	L	L	L		**W4-C**	E	E	E	
S5 (Overall)	N	N	N		**W5-F**	N	N	N	
West	N	N	N		**W6-H**	N	**N**	**L**	OM; RV
East	N	N	N		**W7-D**	N	**E**	**N**	
S6 (Overall)	N	N	N		**W8-G**	N	E	E	
West	N	**N**	**E**		**W9-I**	N	**E**	**N**	RH; RV
East	N	N	N		**E1**	N	**N**	**E**	
S7 (Overall)	N	**N**	**E**	WS	**E2**	N	**N**	**L**	
West	E	**N**	**E**		**E3**	N	N	N	
East	N	**N**	**E**		**NA1**	L	L	L	
S8	E	E	E		**NA2**	N	N	N	
					NA3	L	**N**	**L**	WS
					NA4	N	N	N	

Table A1: Parameter threshold values for the two sets of the OWZ-Detector's detection criteria, subscripts refer to hPa level.

	OWZ-Detector Parameter thresholds					
Criterion	OWZ_{850}	OWZ_{500}	RH_{950}	RH_{700}	$VWS_{850\text{-}200}$	SpH_{950}
Initial	$50 \times 10^{-6} s^{-1}$	$40 \times 10^{-6} s^{-1}$	70%	50%	$25 ms^{-1}$	$10 gkg^{-1}$
Core	$60 \times 10^{-6} s^{-1}$	$50 \times 10^{-6} s^{-1}$	85%	70%	$12.5 ms^{-1}$	$14 gkg^{-1}$